

Article

Morphological and Mechanical Characterization of Films Incorporating Porphyrin Extracted from *Porphyra Dioica*

Ricardo S. Baptista ^{1,2} , Marco Teles ³ , Pedro Adão ⁴ , Clélia Afonso ³ , Raul Bernardino ^{3,5,6} , Susana Bernardino ³, Alberto C. Ferro ^{7,8} , Sara Elias ⁸ and Mafalda Guedes ^{1,8,*} 

- ¹ CDP2T and Department of Mechanical Engineering, Setúbal School of Technology, Instituto Politécnico de Setúbal, 2910-761 Setúbal, Portugal
- ² IDMEC-LAETA, Instituto Superior Técnico, ULisboa, Av. Rovisco Pais 1, 1049-001 Lisboa, Portugal
- ³ MARE, School of Tourism and Maritime Technology, Polytechnic of Leiria, 2520-630 Peniche, Portugal
- ⁴ MARE, Polytechnic of Leiria, 2520-630 Peniche, Portugal
- ⁵ LSRE/LCM Laboratory of Separation and Reaction Engineering—Laboratory of Catalysis and Materials, Polytechnic of Leiria, 2411-901 Leiria, Portugal
- ⁶ ALiCE—Associate Laboratory in Chemical Engineering, Faculty of Engineering, University of Roberto Frias, 4200-465 Porto, Portugal
- ⁷ Department of Mechanical Engineering, Instituto Superior Técnico, ULisboa, Av. Rovisco Pais, 1049-001 Lisboa, Portugal
- ⁸ CeFEMA-LaPMET, Instituto Superior Técnico, ULisboa, Av. Rovisco Pais, 1049-001 Lisboa, Portugal
- * Correspondence: mafalda.guedes@estsetubal.ips.pt

Abstract: This paper studies the effects of glycerol plasticizers and/or alginate, pectin, and carboxymethylcellulose polysaccharides on the mechanical and physical properties of porphyrin-based films to evaluate the films' ability to be used as food packaging. Films were characterized in terms of their composition, microstructural and morphological features, thermal properties, water interaction, and mechanical performance. All films are homogeneous, transparent, and slightly brownish in color. The structures are amorphous and crosslinked, showing the films' thermoset nature. Moisture content and water solubility depend on the second polysaccharide added to the porphyrin, but they both increase with the addition of glycerol to the formulations; water vapor permeability is strongly affected by the second polysaccharide in the formulation. The films display stiff and brittle mechanical behavior, but ductility increases significantly in formulations containing glycerol plasticizers. The barrier and mechanical performance values of the materials produced were found to be lower than those reported for commercial food packaging. The formulations containing glycerol displayed lower water vapor permeability values, ranging from 2.98 for porphyrin/carboxymethylcellulose/glycerol to 6.65 mm·g·d⁻¹·m⁻²·kPa⁻¹ for porphyrin/alginate/glycerol films. All films, except porphyrin/glycerol and porphyrin/alginate/glycerol, had ultimate tensile strengths above 10 MPa—the threshold value that ensures that a package is ductile enough to withstand handling and forming operations. Furthermore, the porphyrin/pectin/glycerol and porphyrin/carboxymethylcellulose/glycerol films displayed sufficiently high ductility values of 2.94 and 3.10%, respectively. These results indicate that the studied porphyrin/pectin/glycerol and porphyrin/carboxymethylcellulose/glycerol formulations have a combination of physical and mechanical properties that ensure adequate film integrity and function through the complete food packaging supply chain. The results here reported represent an opportunity to extend the scope of porphyrin films to applications in the dry food packaging industry.

Keywords: edible food packaging; porphyrin films; glycerol plasticizers; CMC; pectin; alginate; mechanical properties



Citation: Baptista, R.S.; Teles, M.; Adão, P.; Afonso, C.; Bernardino, R.; Bernardino, S.; Ferro, A.C.; Elias, S.; Guedes, M. Morphological and Mechanical Characterization of Films Incorporating Porphyrin Extracted from *Porphyra Dioica*. *Coatings* **2022**, *12*, 1720. <https://doi.org/10.3390/coatings12111720>

Academic Editor: Maria Jose Fabra

Received: 11 October 2022

Accepted: 2 November 2022

Published: 10 November 2022

Publisher's Note: MDPI stays neutral with regard to jurisdictional claims in published maps and institutional affiliations.



Copyright: © 2022 by the authors. Licensee MDPI, Basel, Switzerland. This article is an open access article distributed under the terms and conditions of the Creative Commons Attribution (CC BY) license (<https://creativecommons.org/licenses/by/4.0/>).

1. Introduction

Food packaging serves as an enclosure envisaged to contain and protect food products and to provide consumers with information about ingredients and nutrition [1]. It

is thus an essential factor in the food supply chain, from processing through to handling, transportation, and display [2]. Food packaging must establish a physical protective barrier against the main external factors that accelerate food degradation, including biological (microorganisms and insects), chemical (e.g., oxygen, carbon dioxide, moisture), and physical agents (e.g., impact and vibration during transport) [1,3]. Conventional food packaging materials include glass, metal, paper, plastic, and their composites, with corresponding advantages and limitations [1,3]. Packaging metals and glasses have high formability and are ideal recycling materials, being easily reclaimed and processed into new products [1]. However, they have high density values, and heavy weight adds to transportation costs; glass is brittle and susceptible to fracture; metals are expensive compared to other packing materials [1,3]. Paper is cheap and biodegradable but offers weak barrier properties; food-grade paper must almost always be treated, coated, laminated, or impregnated with waxes, resins, or lacquers to improve functional and protective properties, resulting in increased costs and hindered recyclability [1]. Plastics are inexpensive, easily formed, chemically resistant, lightweight, and offer sufficient physical barrier against gases and vapors for short-time protection [1,3]. However, thermosets are not recyclable, and thermoplastics (although recyclable) present huge practical limitations with respect to their separation into valuable waste fractions [1]; also, plastic waste is associated with high emissions of carbon dioxide and other greenhouse gases during incineration and with ocean and landscape contamination in the case of microplastics [2,3]. Despite the identified environmental problems (especially when considering single-use films and coatings for the protection of fast-consumption products), the use of plastics in food packaging is ubiquitous and rising [2], promoted by their low costs and functional advantages over traditional materials (e.g., thermosealability, microwavability) [3]. New packaging systems based on edible, biodegradable, and/or compostable materials have been developed as means of limiting the use of persistent plastics [4]. Biopolymers extracted from plant and animal sources or derived from natural polymers can be used for this purpose [1,2] and have been developed into actual commercial products in the last few years [4]. In particular, polysaccharides from macroalgae (mostly alginates, carrageenans, and agar) are being increasingly used for the formulation of edible packaging, either alone or combined with other biopolymers [4–6]. Such packaging can be used in the form of wraps, pouches, and coatings, but despite current technological advances and conversion processes, further progress is still required regarding their poor mechanical and barrier properties [2,4,7].

In this context, the current authors have been developing novel biodegradable edible films based on porphyran extract isolated from the red macroalgae *Porphyra dioica* [8]. Porphyran is an anionic, water-soluble polysaccharide, with a linear backbone and a very complex structure consisting of repeating arrangements of D-galactose and L-galactose-sulfate units in alternating sequence (Figure 1a), disturbed by the partial substitution of D-galactose by methylether (Figure 1b) and of L-galactose-sulphate by anhydrous-L-galactose (Figure 1c) [7,9]. The proportions of these components vary widely from sample to sample, with those of sulfated ester ranging from 6 to 11% and those of 6-anhydrogalactose from 5 to 19% [10].

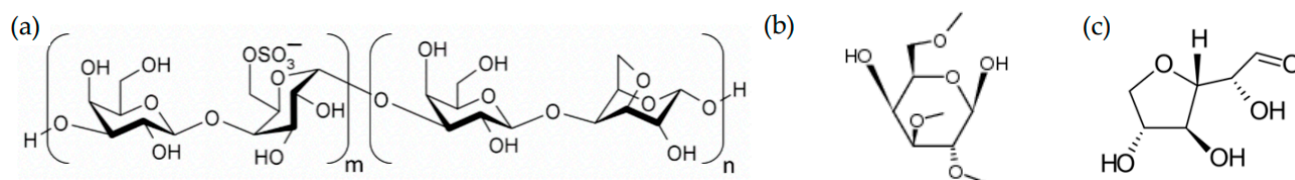


Figure 1. Structural units in porphyran. (a) Idealized structure, where the main repeating units are (L-galactose-sulphate (m), and D-galactose (n)) [11]. Residues present: (b) methylether and (c) anhydrous-L-galactose [7].

Although the precise composition depends on algal species and genus and shows seasonal and environmental variation [12], red macroalgae contain around 40% polysac-

charides [13], from which up to more than 80% are porphyran [10]. Porphyran thus stands as an abundant and sustainable resource that, additionally, does not compete with food production or food security [4]. In addition, since porphyran has a high viscosity and a basic structure closely related to that of agarose (which displays excellent gelling properties), a strong filmogenic ability is to be expected [10]. Overall, this suggests potential for a new generation of food packaging films based on porphyran [13]. In practice, however, the high amount of sulfate present in the structure (6–11%) (Figure 1a) prevents gel formation, because the resulting high electrostatic repulsion among porphyran chains hinders their association, binding, and crosslinking [10]. For this reason, although recognized as a valuable polymer for applications in the pharmaceutical and cosmetic industries [11], porphyran has not been used in the food industry [10]. Gelation can, however, be induced by desulfation, which decreases electrostatic repulsion among chains, allowing interactions through non-covalent bonds (hydrophobic interactions or electrostatic interactions via hydroxyl groups) [10,14]. Excellent gelation and filmogenic properties can thus be developed [8,10,14], such that porphyran has potential for use as a gelling agent in edible food packaging films. Furthermore, the antioxidant and anti-inflammatory properties that have been shown by its use in pharmacy and cosmetics [4,14,15] are potentially very useful for extending the shelf lives of contained food products. However, to the best of the authors' knowledge, only a small number of reports are available regarding its application in food packaging [16–19]. Bearing this in mind, porphyran-based films for edible packaging were envisioned and produced in a previous work [8]. A porphyran biopolymer was used as a matrix after extraction and water was used as the solvent. In order to improve structural cohesion, the incorporation of other food-grade polysaccharides—amidated pectin, sodium alginate, and sodium carboxymethylcellulose—was tested [4]; glycerol was used as a plasticizer to increase the films' flexibility [4]. The suitability of the produced porphyran-based films from chemical, toxicity, durability, and organoleptic standpoints was previously established [8]. The materials also display antioxidant properties [8]. Given these attributes, films' application in packaging for dry food, in which lipid oxidation and water absorption are the main factors responsible for shelf-life reduction, was envisaged. Although these characteristics indicate their chemical suitability to be used as packaging, information regarding films' endurance to physical agents is still to be obtained. This information is crucial to ensure packaging integrity during the full chain, from production through to storage and distribution. For this reason, the current paper studies barrier properties, and mechanical performance in order to complete films' characterization.

2. Materials and Methods

2.1. Film Formulation and Processing

The films tested in the current paper were previously formulated and produced; the extraction, filmogenic solution preparation, and film forming process have been thoroughly described elsewhere [8]. Briefly, semi-refined porphyran extract was obtained from *Porphyra dioica* (ALGAplus; purity > 95%, moisture $\leq 12 \pm 3\%$) using a Soxhlet extractor and a green solvent (hot water). The extract was then used to produce the porphyran-based films, using a casting process adapted from [20]. Besides a non-added reference solution (PorphSR), formulations also containing sodium carboxymethylcellulose (CMC), pectin (PcT), or sodium alginate (AL) were also produced. Table 1 describes the used reagents, which were all food-grade in order to maintain the edible quality of the resulting materials [4]. The polysaccharides were dissolved in distilled water at 100 °C in the proportions described in Table 2. After complete dissolution, the solutions were filtered under vacuum. Glycerol was then added, when applicable, and the resulting filmogenic solutions remained under magnetic mixing at 100 °C for 2 h.

Table 1. Reagents used in the filmogenic solutions (according to supplier, except when mentioned). All reagents were food-grade.

| Reagent (Supplier) | d (g/cm ³) | Chemical Composition (wt%) | Observations |
|---------------------------------------|------------------------|--|---|
| Porphyran extract [8] | 1.5 | 67.7% D-galactose undetectable protein contamination | Anionic polysaccharide [10]. Gelling properties and film-forming potential after suitable chemical treatment [2,10,21]. T _g between 35–38 °C [14]. |
| Sodium alginate (BDH) | 1.601 | n.a. | Anionic polysaccharide based on the sodium salt of alginic acid. Low water barrier properties [2]. |
| Sodium carboxymethylcellulose (Sigma) | 1.59 | Degree of anhydroglucose substitution by carboxymethyl: 65–90 Na = 6.5–9.5 | Water-soluble, anionic polysaccharide with gelling, thickening, moisture retention, emulsification, and stabilization ability [2,22] |
| Amidated pectin (BioSynth) | 1.16–1.50 [23] | Degree of amidation: 10–16 Degree of esterification: 32–40 Contains β-TCP, SAPP and glyucose | Anionic polysaccharide with galacturonic acid backbone. Gelling, thickening, moisture retention, emulsification, stabilization ability [2,22]. Antioxidant and antimicrobial abilities [23] |
| Glycerol (ThermoFisher) | 1.226 | Impurities ≤ 0.0047 H ₂ O = 13.3 Glycerol = 86.9 | Plasticizer agent [2]. T _g = 78 °C; T _{decomposition} > 290 °C [24] |

d: density; LOI: loss on ignition; M: molecular weight; n: polymerization degree; n.a.: not available; SAPP: disodium pyrophosphate; TCP: tricalcium phosphate; T_g: glass transition temperature.

Table 2. Solid contents and compositions (based on dry weight) of the produced porphyran-based solutions, calculated from [8].

| Film | Solid Load (wt%) | Porphyran (wt%) | CMC (wt%) | PcT (wt%) | AL (wt%) | Glycerol (wt%) | Porphyran/ Polysaccharide * (wt ratio) | Glycerol/ Polysaccharides ** (wt ratio) |
|-----------------|------------------|-----------------|-----------|-----------|----------|----------------|--|---|
| PorphSR | 1.0 | 100.0 | | | | | 1/0 | |
| PorphSR_Gly | 1.1 | 87.3 | | | | 12.7 | 1/0 | 1/6.9 |
| PorphSR_CMC | 2.0 | 46.8 | 53.2 | | | | 1/1.1 | |
| PorphSR_CMC_Gly | 2.1 | 43.8 | 49.8 | | | 6.4 | 1/1.1 | 1/14.7 |
| PorphSR_PcT | 1.0 | 46.8 | | 53.2 | | | 1/1.1 | |
| PorphSR_PcT_Gly | 1.2 | 43.8 | | 49.8 | | 6.4 | 1/1.1 | 1/14.7 |
| PorphSR_AL | 1.5 | 30.6 | | | 69.4 | | 1/2.3 | |
| PorphSR_AL_Gly | 1.6 | 28.1 | | | 63.8 | 8.1 | 1/2.3 | 1/11.3 |

AL: sodium alginate; CMC: sodium carboxymethylcellulose; Gly: glycerol; PcT: pectin; SR: semi-refined porphyran extracted by the Soxhlet method. * Added polysaccharide, excluding porphyran. ** Total polysaccharides, including porphyran.

The prepared filmogenic solutions were then slip-casted in 56.74 cm² circular molds. For each solution, 25 mL was casted per mold (corresponding to 0.44 mL/cm²) and dried under vacuum (40 °C, 18–20 h) to obtain a solid film [8]. The mold was then placed on a surface at approximately 60 °C, and the film was removed. For comparison purposes, a commercial polymeric film (with unknown composition) used in the packaging of chocolate breakfast cereals (Dia Chocolate Balls, Dia, Las Rozas, Madrid, Spain) was used as reference.

Films were characterized regarding moisture content according to ASTM D644-00:2004. After initial weight (w_0) measurement, the samples were dried in an oven at 105 °C for 24 h. The final weights (w_f) were determined, and the films' moisture content (MC) were

calculated using Equation (1). Each reported value represents the mean value of at least 3 samples taken from different films of each composition.

$$MC = \frac{w_0 - w_f}{w_0} \times 100 \quad (1)$$

2.2. Morphological Characterization

The microstructural features of the produced films were characterized using field emission scanning electron microscopy (FEG-SEM) (JEOL JSM-7001F) coupled to energy dispersive spectroscopy microanalysis (EDS) (Oxford Instruments Inca pentaFETx3). Samples were previously coated with a Au-Pd alloy to avoid an accumulation of electrical charge during observation. EDS microanalysis was carried out upon uncoated samples. Circular samples (\varnothing 8 mm) were used to assess film thickness. Samples were previously weighed on an analytical balance (AND 200), and density was measured via the Archimedes method by immersion in absolute ethanol (Fisher Chemical, $d = 0.789 \text{ g/cm}^3$); the obtained density values were used to calculate thicknesses. Four samples of each composition were tested for reproducibility assessment. Surface roughness was measured by laser profilometry (Profil3D). The presence of crystalline phases in the films was studied by X-ray diffraction (XRD) (BRUKER D8 Advance) using $\text{CuK}\alpha$ radiation, 2θ range between 10 and 50° , step size of 0.02° , and step time of 2 s. Morphological observations and measurements were carried out on the film surfaces that dried freely.

2.3. Thermal Characterization

The onset temperature of film softening, and thermal degradation was assessed by differential scanning calorimetry (DSC) (NETZSCH 200F3 Maia). Samples were heated to 280°C , cooled to 20°C (using liquid nitrogen) and reheated to 280°C . Heating and cooling took place at $10^\circ\text{C}/\text{min}$, under nitrogen gas flow ($50 \text{ mL}/\text{min}$). Samples (3–5 mg) were placed in covered aluminum pans; an empty pan was used as a reference. At least three tests were carried out for each material for reproducibility.

2.4. Characterization of Film Interactions with Water

Film solubility in water was determined using the method proposed by Kanmani and co-workers [25] ilm samples were dried at 100°C for 24 h, their initial weights (w_0) were measured, and they were immersed in distilled water under magnetic stirring. After 8 h, the beaker contents were filtered, and the retained fractions were dried at 100°C for 24 h, after which final weights (w_f) were measured. Solubility in water (WS) was calculated using Equation (2) [18], where MC is the moisture content (Equation (1)). WS tests were carried out in triplicate.

$$WS = \frac{w_0 \times (100 - MC) - w_f}{w_0 \times (100 - MC)} \times 100 \quad (2)$$

The ability of the produced films to function as water vapor barrier was measured using the desiccant method specified in ASTM E96–95. Each film was used to seal the open mouth of a test beaker containing silica gel desiccant (LabKem) and placed in a controlled atmosphere (30°C , 50% relative humidity). Periodic weighting was carried out over 48 h. Changes in weight (G) were recorded and plotted as functions of elapsed time (t). The slope of the straight line that adequately fitted the plot when steady-state conditions were reached was obtained by linear regression (G/t), and the water vapor transmission rate (WVTR) was calculated by dividing by the test area (A) (Equation (3)). Water vapor permeability (WVP) was then calculated using Equation 4, where d is the film thickness and ΔP is the water vapor pressure differential (4245 Pa at 30°C) between the oven headspace and the fully dry environment provided by the silica gel inside the beaker [25,26]. The

reported values represent the mean values of at least 3 samples taken from different films of each composition.

$$WVTR = \frac{G}{tA} \quad (3)$$

$$WVP = d \frac{WVTR}{\Delta P} \quad (4)$$

2.5. Mechanical Testing

Tensile tests were carried out on a universal electromechanical testing machine (INSTRON 5544) equipped with a 100 N load cell (INSTRON) and a video strain gauge (INSTRON SVE I). Tests proceeded until sample fracture, with an elongation rate of 1 mm/min. Films' apparent Young's modulus (E'), ultimate tensile stress (UTS), and fracture strain (ϵ_f) were calculated according to ASTM D638. At least 3 ($n = 3 - 6$) samples of 15 mm width, 95 mm length, and 55 mm gauge length were tested per film composition.

3. Results

3.1. Film Morphology

The obtained macrographs indicate that the produced films are even and smooth, although showing some waviness (Figure 2). The films are transparent, displaying a light brown shade in the absence of glycerol (Figure 2a–d) and a slightly darker hue when the plasticizer is present (Figure 2e–h). The formulations containing two polysaccharides yielded a homogeneous layer in all cases (Figures 2b–d and 2f–h). All the films are sufficiently strong and flexible to resist manipulation, observation, and analysis, showing the ability of the developed materials to form continuous layers by mold casting.

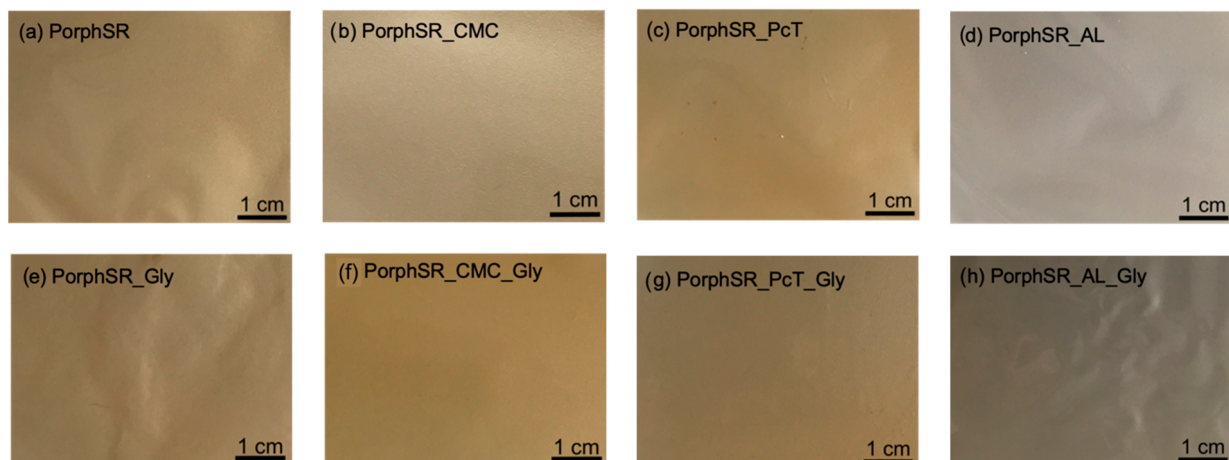


Figure 2. Macroscopic features of the produced films. Without added glycerol: (a) PorphSR; (b) PorphSR_CMC; (c) PorphSR_PcT; (d) PorphSR_AL. With added glycerol: (e) PorphSR_Gly; (f) PorphSR_CMC_Gly; (g) PorphSR_PcT_Gly; (h) PorphSR_AL_Gly.

While the films appeared dense, uniform, homogeneous, and defect-free at the macroscale, FEG-SEM observations highlighted important microstructural differences, both in films without (Figure 3a–d) and with (Figure 3e–h) glycerol.

PorphSR (Figure 3a) apparently displayed the most uniform microstructure and smoothest surface among all the produced films. In the absence of glycerol, film surface roughness (Figure 4a, dashed line) successively increased when CMC (Figure 3b), pectin (Figure 3c), and alginate (Figure 3d) were blended in. The addition of glycerol apparently improved sample uniformity, with fewer entrapped bubbles (Figure 3e–h) and lower surface roughness (Figure 4a, full line) when compared with the corresponding glycerol-free film. The addition of glycerol also appeared to decrease film thickness (Figure 4b, full line) compared to compositions without plasticizers (Figure 4b, dashed line). Film

thickness varied between approximately 30 (PorphSR) and 44 μm (PorphSR_AL) in the absence of glycerol and between around 28 (PorphSR_Gly) and 43 μm (PorphSR_A_Gly) in blends containing glycerol. These values are an order of magnitude lower than the measured thickness of the reference commercial film, $393.3 \pm 4.1 \mu\text{m}$. The density value of the produced materials ranged between 1.45 (PorphSR_PcT) and 1.63 g/cm^3 (PorphSR_AL) in compositions without glycerol plasticizers (Figure 4c, dashed line). In comparison, the density values of the respective compositions blended with glycerol (Figure 4c, full line) were lower, ranging between a minimum of 1.37 (PorphSR_PcT) and 1.61 g/cm^3 (PorphSR_AL_Gly). The attained values were in good agreement with values calculated using the rule of mixtures (density values of raw materials in Table 1). The density values of the produced materials were 40 (PorphSR_PcT) to 70% (PorphSR_AL) higher than the measured density value of the reference commercial film, $0.96 \pm 0.4 \text{ g/cm}^3$ (Table 1).

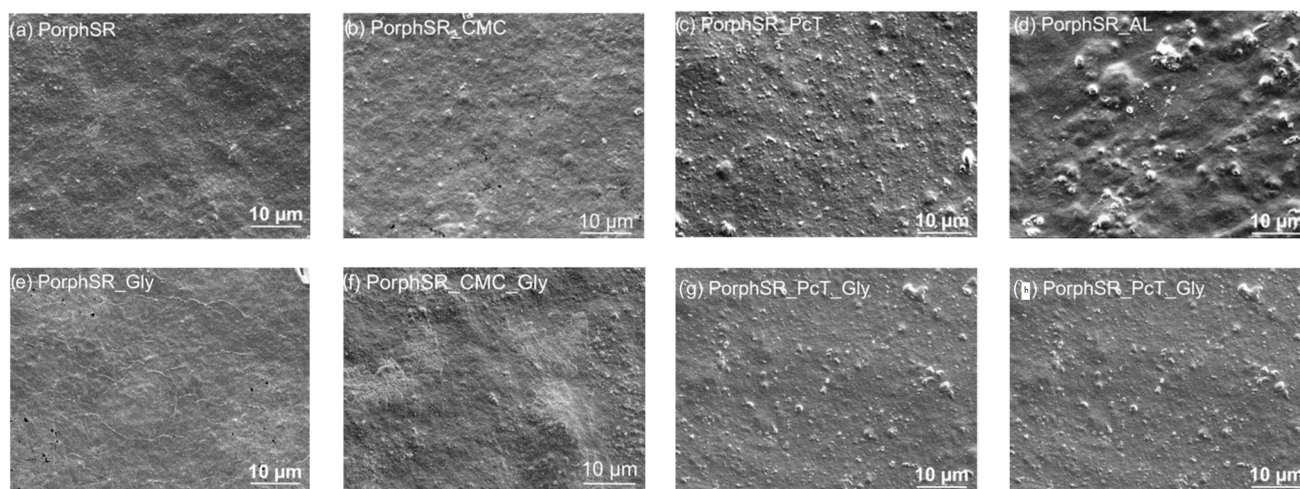


Figure 3. SEM images of the produced films. Without added glycerol: (a) PorphSR; (b) PorphSR_CMC; (c) PorphSR_PcT; (d) PorphSR_AL. With added glycerol: (e) PorphSR_Gly; (f) PorphSR_CMC_Gly; (g) PorphSR_PcT_Gly; (h) PorphSR_AL_Gly.

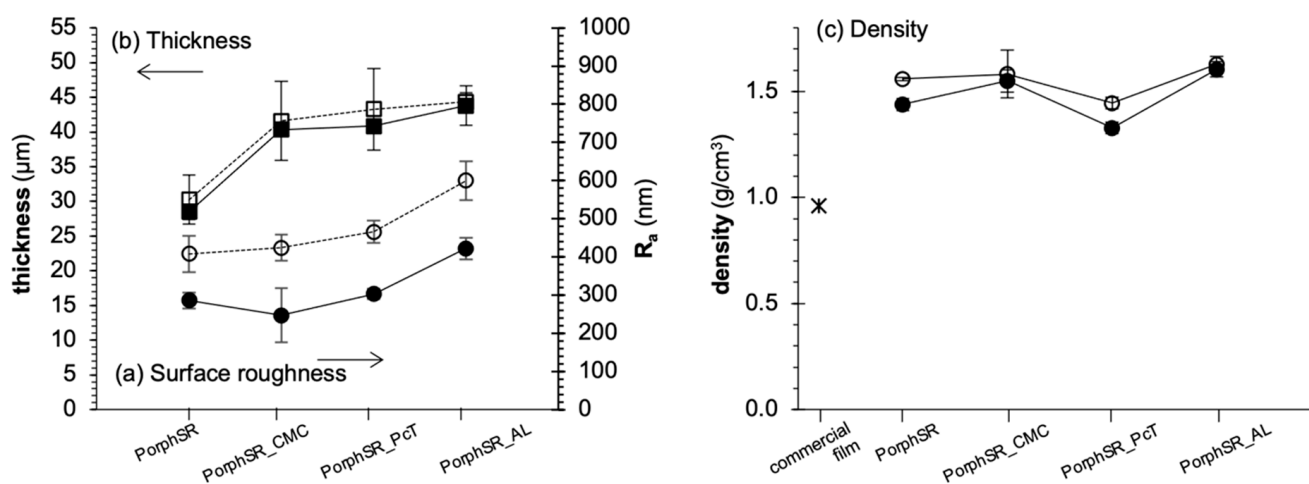


Figure 4. Measured morphological features of the produced films: (a) arithmetic mean surface roughness (R_a); (b) film thickness; (c) material density. (Clear symbols: compositions without glycerol; full symbols: samples with glycerol; *: reference commercial film.)

3.2. Film Composition

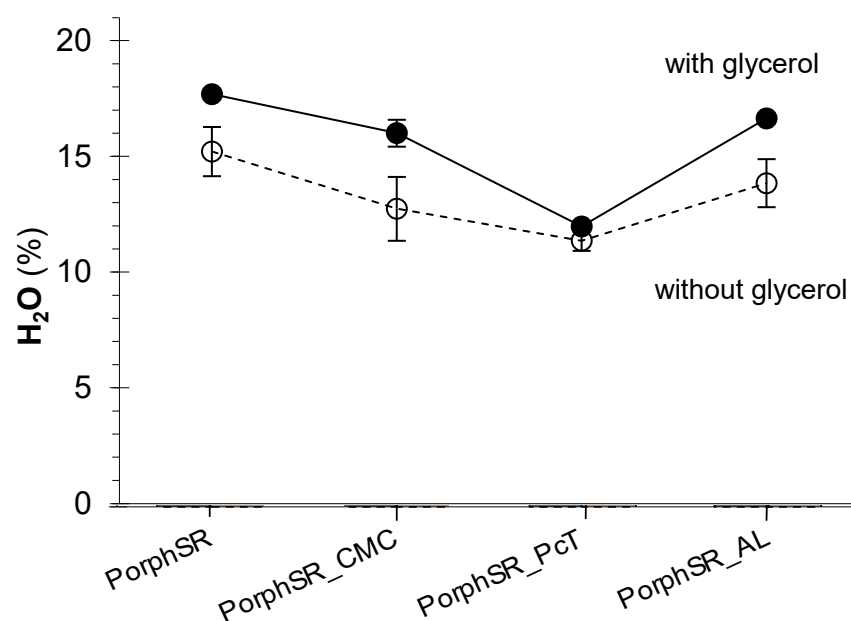
Table 3 displays the semiquantitative elemental compositions of the produced films determined by microanalysis.

Table 3. Element/carbon ratio on the produced films, obtained by semiquantitative microanalysis (hydrogen atomic number is below the EDS equipment detection ability, preventing its quantification).

| Elements (at/at) | PorphSR | PorphSR_Gly | PorphSR_CMC | PorphSR_CMC_Gly | PorphSR_PcT | PorphSR_PcT_Gly | PorphSR_AL | PorphSR_AL_Gly |
|------------------|-------------|-------------|-------------|-----------------|-------------|-----------------|-------------|----------------|
| N/C | 0.15 ± 0.00 | 0.08 ± 0.00 | 0.05 ± 0.00 | 0.05 ± 0.00 | 0.09 ± 0.00 | 0.09 ± 0.00 | 0.05 ± 0.00 | 0.08 ± 0.00 |
| O/C | 1.22 ± 0.03 | 1.34 ± 0.03 | 0.83 ± 0.02 | 1.13 ± 0.02 | 0.79 ± 0.02 | 0.81 ± 0.02 | 1.12 ± 0.02 | 0.93 ± 0.02 |
| Na/C | 0.22 ± 0.01 | 0.10 ± 0.03 | 0.19 ± 0.02 | 0.18 ± 0.02 | 0.13 ± 0.02 | 0.09 ± 0.02 | 0.20 ± 0.02 | 0.09 ± 0.02 |
| Mg/C | 0.02 ± 0.00 | 0.02 ± 0.00 | 0.01 ± 0.00 | 0.01 ± 0.00 | 0.01 ± 0.00 | 0.01 ± 0.00 | 0.01 ± 0.00 | 0.01 ± 0.00 |
| P/C | 0.02 ± 0.00 | 0.02 ± 0.00 | 0.01 ± 0.00 | 0.01 ± 0.00 | 0.03 ± 0.00 | 0.05 ± 0.00 | 0.01 ± 0.00 | 0.10 ± 0.00 |
| S/C | 0.19 ± 0.00 | 0.11 ± 0.00 | 0.04 ± 0.00 | 0.07 ± 0.00 | 0.04 ± 0.00 | 0.03 ± 0.00 | 0.03 ± 0.00 | 0.08 ± 0.00 |
| Cl/C | 0.05 ± 0.01 | 0.02 ± 0.00 | | 0.04 ± 0.00 | | 0.01 ± 0.00 | | 0.01 ± 0.00 |
| K/C | 0.25 ± 0.00 | 0.12 ± 0.00 | 0.03 ± 0.00 | 0.08 ± 0.00 | 0.03 ± 0.00 | 0.03 ± 0.00 | 0.02 ± 0.00 | 0.05 ± 0.00 |
| Ca/C | 0.01 ± 0.00 | 0.01 ± 0.00 | | 0.01 ± 0.00 | 0.01 ± 0.00 | 0.01 ± 0.00 | | 0.02 ± 0.00 |

Films' composition was found to be in overall agreement with the compositions of the corresponding raw materials (Table 1), mainly containing C and O, together with smaller amounts of N, Na, S, K, P, and Ca [8]. Cl was identified in the PorphSR, PorphSR_Gly, PorphSR_CMC_Gly, PorphSR_PcT, and PorphSR_PcT_Gly films, although it was not present in the raw materials, and none of the processing steps involved the presence of chlorinated reagents [8]. Its presence is expected to have resulted from marine atmospheric contamination during film storage before testing (the lab is in a marine environment).

The determined H₂O contents (Figure 5) were consistently higher in films with plasticizers: they ranged from 11.4 wt% (PorphSR_PcT) to 15.1 wt% (PorphSR) in films without glycerol and from 12.0 wt% (PorphSR_PcT_Gly) to 19.7 wt% (PorphSR_Gly) in the corresponding film with glycerol. The difference in moisture content due to the presence of glycerol was maximum in the plain PorphSR system (an approximately 30% increase when glycerol was added) and minimum in the PcT system (5.4%). Moisture content increase in the presence of glycerol is expected to result from its highly hydrophilic and hygroscopic nature [22].

**Figure 5.** Moisture contents (Equation (1)) in the produced films. (Clear symbols: compositions without glycerol; full symbols: compositions with glycerol.)

XRD results (Figure 6) confirmed the amorphous character of the produced films. The attained diffractograms displayed broad features, high initial backgrounds, and high noise, consistent with incoherent scattering from amorphous solids [24]. Nevertheless, a small number of low-intensity diffraction peaks is present in some of the materials. In PorphSR films (Figure 6a), the reference's most intense galactose diffraction peak at 18.1° was present as a broad bulge, indicating the amorphous character of the material [27–30]; the well-defined peaks at 14.0 and 28.2° and the lower intensity peaks at 13.4 , 16.2 , 20.3 , and 29.1° also matched crystalline galactose (ICDD 09-0620). When glycerol was added to the system (PorphSR_Gly films, Figure 6b), the number and intensity of galactose peaks decreased compared to PorphSR. In PorphSR_AL_Gly films (Figure 6h), no diffraction peaks were detected. Finally, in PorphSR_CMC (Figure 6c) and PorphSR_CMC_Gly (Figure 6d), PorphSR_PcT (Figure 6e) and PorphSR_PcT_Gly (Figure 6f), and also in PorphSR_AL (Figure 6g) the diffractograms only displayed a broad background blunt around the 2θ position corresponding to the most intense peaks of the crystalline phase (around 20° for CMC [29], 14 and 21° for pectin [31], and 14° for sodium alginate [32]). In all cases, the presence of broad blunts instead of well-defined peaks is indicative of amorphous structures [27,29,30]. Blending individual porphyran with CMC (PorphSR_CMC, Figure 6c) or pectin (PorphSR_PcT, Figure 6e) resulted in peak elimination, indicating that phase miscibility in the filmogenic medium is higher in the blends [29]. The presence of glycerol plasticizers introduced a similar effect, eliminating the alginate peak in PorphSR_AL_Gly (Figure 6h) and decreasing the number and intensity of galactose peaks present in PorphSR_Gly (Figure 6b). It should be mentioned that the main NaCl diffraction peak (31.7°) was identified in all materials, except PorphSR_CMC, PorphSR_AL, and PorphSR_AL_Gly. This matches CI detections in some of the films (Table 3), resulting probably from the aforementioned atmospheric contamination (§3.2).

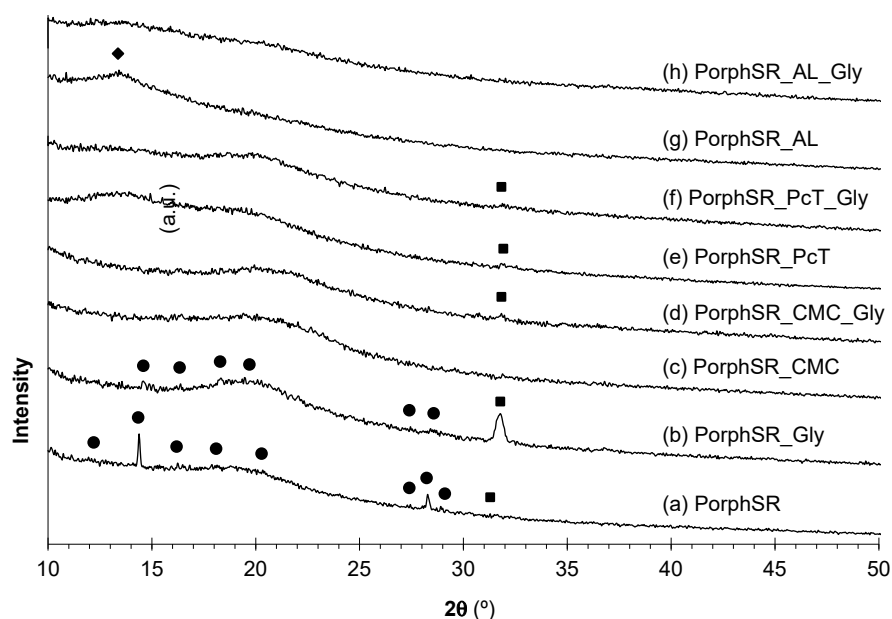


Figure 6. Diffractograms obtained for porphyran-based films: (a) PorphSR; (b) PorphSR_Gly; (c) PorphSR_CMC; (d) PorphSR_CMC_Gly; (e) PorphSR_PcT; (f) PorphSR_PcT_Gly; (g) PorphSR_AL; (h) PorphSR_AL_Gly. (● galactose, ICDD 09-0620; ■ NaCl, ICDD 01-0994; ◆ alginate [32].)

3.3. Thermal Properties

The obtained DSC plots are presented in Figure 7. During the first heating run, films without (Figure 7a–d) and with glycerol (Figure 7e–h) display one endothermic event and two well-defined endothermic peaks, followed by a broad exothermic peak. The first corresponds to glass transition, indicating that cooperative movement of polymer chains was still possible and underlining that the produced films were not fully cross-linked [33]. Glass

transition onset (Figure 7i) ranged from approximately 45 °C (PorphSR_CMC) to 57 °C (PorphSR) in films without glycerol and from approximately 31 °C (PorphSR_PcT_Gly) to 40 °C (PorphSR_Gly) when glycerol is present.

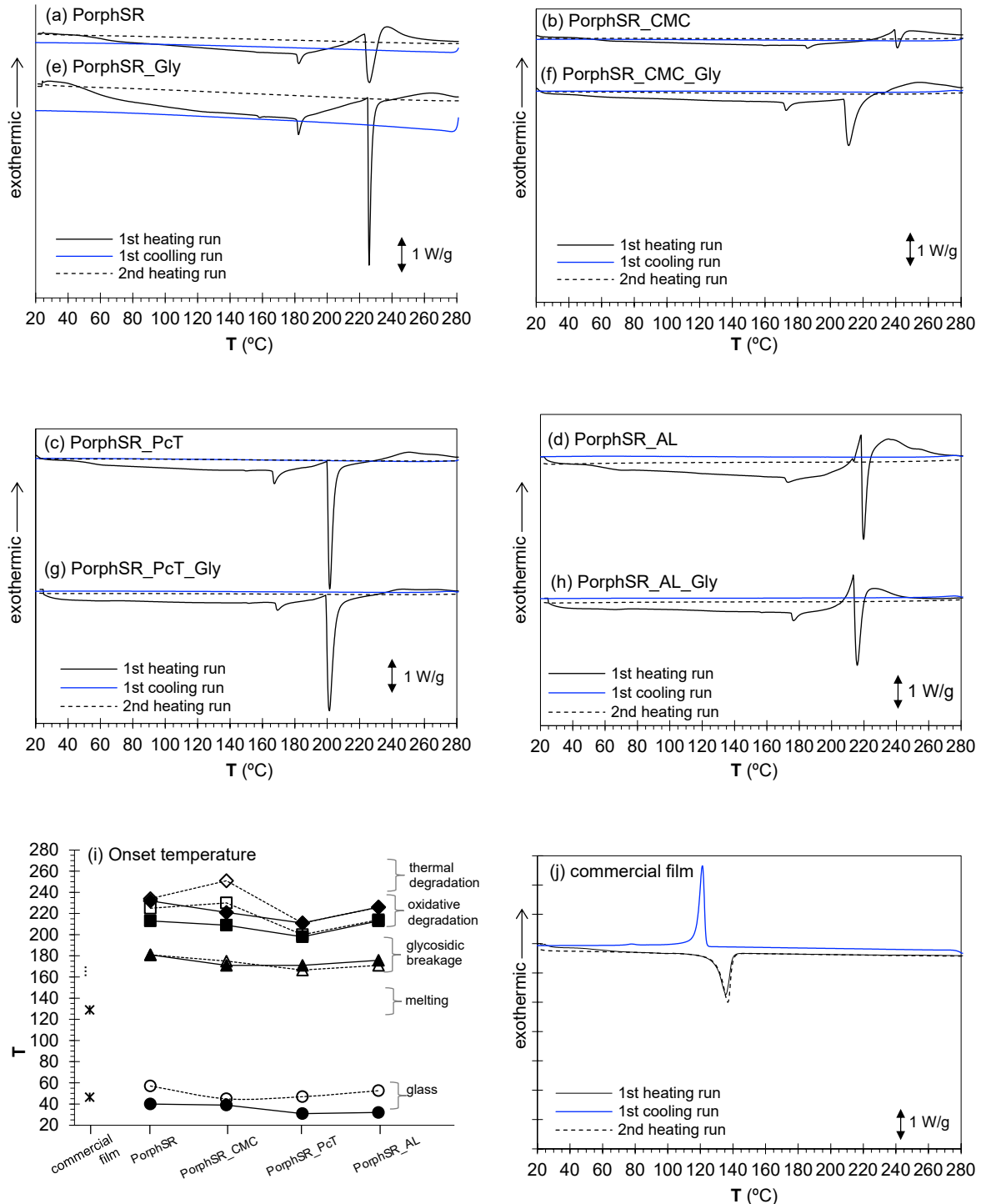


Figure 7. DSC plots of (a) PorphSR, (b) PorphSR_CMC, (c) PorphSR_PcT, and (d) PorphSR_AL films. Effects of the presence of plasticizers on thermal behavior: (e) PorphSR_Gly, (f) PorphSR_CMC_Gly, (g) PorphSR_PcT_Gly, and (h) PorphSR_AL_Gly films. (i) Onset temperature of thermal events in the produced films. (Clear symbols: compositions without glycerol; full symbols: compositions with glycerol; *: reference commercial film.) (j) DSC plot of the reference commercial film.

The endothermic peaks are expected to correspond to the decomposition of the porphyrin polysaccharide [34]. Polysaccharide pyrolysis begins by the random breaking of glycosidic bonds, followed by further decomposition. In good agreement with this, the endothermic peak at lower temperatures has been previously assigned to the breakage of the β -1,4-glycosidic bonds between 1,3-linked β -d-galactosyl units and α -l-galactosyl 6-sulfate units of porphyrin main chains [35]. The second corresponds to the activation energy for the onset of oxidative decomposition [34]. In the produced materials, glycosidic breakage onset was detected between 167 and 185 °C, depending on composition. In PorphSR-, PorphSR_PcT-, and PorphSR_AL-based materials, the onset temperature was similar without and with glycerol (decreasing below 2.5%) (Figure 7i). However, in the PorphSR_CMC-based system it decreases from 185 to 171 °C (approximately 7.6%) when glycerol is present. The onset of oxidative decomposition displayed a similar trend, taking place around 224, 199, and 213 °C for both compositions in the PorphSR-, PorphSR_PcT-, and PorphSR_AL-based systems; in PorphSR_CMC, it decreases from 240 to 209 °C (approximately 13%) when glycerol is present. Furthermore, thermal decomposition, corresponding to the broad and shallow exothermic peak occurring at higher temperature values [15,34], has onset between 211 and 251 °C, depending on composition. In good agreement with the values in Figure 7i, temperatures of approximately 175 and 240 °C have been reported for *Porphyra* algae [15], while full exothermic thermal decomposition is to be expected above around 345 °C [15,34].

The thermograms registered on sample cooling (Figure 7a–h, blue line) and on a second heating run (Figure 7a–h, dashed line) were similar, showing almost straight lines without peaks or baseline shifts. This indicates that the physical transitions (glass transition and eventual crystallization and melting) and chemical reactions (glycosidic breakage and oxidative decomposition) that occurred during the first heating cycle are irreversible and that no structural recovery occurred on cooling. The temperature-imposed irreversible changes revealed the thermoset structures of the produced polymers [33,36]. Remarkably, the reference commercial film displays glass transition (onset at approximately 49 °C) and melting (onset at approximately 129 °C) on heating (Figure 7j, full black line) and totally reforms on cooling (Figure 7i, blue line), rendering a second heating plot (Figure 7j, dashed line) very similar to the first one. These are typical thermal features of semi-crystalline thermoplastics [33].

3.4. Interactions with Water

Only the films with glycerol could be tested for barrier properties, because although all films are flexible and handleable (§3.1), those without glycerol fractured when bent to seal the beaker mouth according to ASTM E96–95 specification and could not be tested. The protection offered by the films can be qualitatively assessed by reference to Figure 8, which shows desiccant weight gain (G) with time for the several films over 48 h.

Overall, the uncovered silica, exposed to oven conditions, absorbed the most water, corresponding to a weight gain of around 12% (Table 4) ($p < 0.001$). Oppositely, the commercial reference film only allowed water transmission corresponding to a 0.8% increase in desiccant weight. Although they did not reach such low values, the produced materials allowed the silica gel to sustain a state of dryness inside the beaker requiring a weight gain varying between only 3 and 6%, confirming their barrier abilities against water vapor. Very strong to evident statistically significant differences were found between all produced materials and the commercial film ($p < 0.05$). The fully detailed statistical analysis in Appendix A (Tables A1–A4) also show statistically significant evidence of distinct behavioural differences between the PorphSR_CMC_Gly (3.07%) and PorphSR_PcT_Gly (5.7%) films. All systems reached stationary conditions after around 10.5 h, and the slope of the corresponding straight line was used to calculate films' WVTR and WVP (Table 4). The produced films displayed water vapor transmission rate values between 315 and 644 $\text{g}\cdot\text{d}^{-1}\cdot\text{m}^{-2}$, i.e., two orders of magnitude higher than the reference film (around 3.4 $\text{g}\cdot\text{d}^{-1}\cdot\text{m}^{-2}$) ($p < 0.001$). The base PorphSR film allows water vapor transportation at a

rate of approximately $444 \text{ g}\cdot\text{d}^{-1}\cdot\text{m}^{-2}$. This value slightly decreased ($415 \text{ g}\cdot\text{d}^{-1}\cdot\text{m}^{-2}$, corresponding to 6.4%) when CMC was present in the formulation (Porph_CMC_Gly) ($p < 0.001$). On the other hand, the presence of pectin (Porph_PcT_Gly) and alginate (Porph_AL_Gly) increased the WVTR to 628 and 644 ($p < 0.001$), respectively, which roughly corresponded to a 40% increase, i.e., water vapor barrier properties are enhanced by the presence of CMC, while the other polysaccharides (PcT and AL) degrade them when compared to PorphSR.

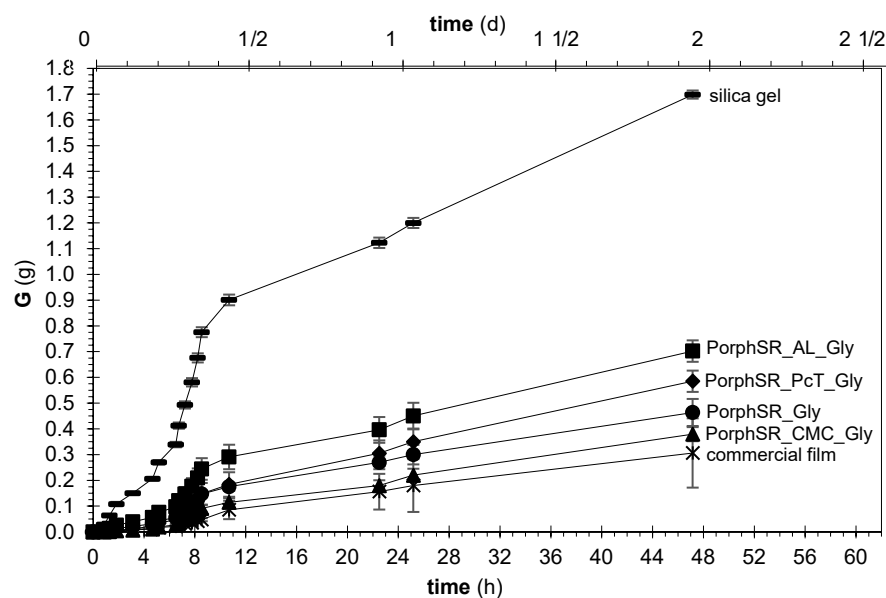


Figure 8. Water barrier effect: cumulative desiccant mass gain (G) over time for the produced materials and for the reference commercial film. The curve attained for uncovered silica gel is also shown. The steady-state slope of each curve was used to calculate the corresponding material WVTR (Equation (3)).

Table 4. Water vapor barrier properties and water solubility of the tested films.

| Film Formulation | Desiccant Weight Gain (%) | Film | | |
|---------------------------|----------------------------------|---|--|--------------------|
| | | WVTR ($\text{g}\cdot\text{d}^{-1}\cdot\text{m}^{-2}$) | WVP ($\text{mm}\cdot\text{g}\cdot\text{d}^{-1}\cdot\text{m}^{-2}\cdot\text{kPa}^{-1}$) | Solubility (%) |
| PorphSR | - | - | - | 100.0 ± 0.0 |
| PorphSR_Gly | 3.64 ± 0.37 | 443.77 ± 4.62 | 2.98 ± 0.10 | 100.0 ± 0.0 |
| PorphSR_AL | - | - | - | 98.8 ± 1.2 (a),(b) |
| PorphSR_AL_Gly | 4.32 ± 1.59 | 644.38 ± 13.86 (b) | 6.65 ± 0.12 (b) | 99.4 ± 0.1 |
| PorphSR_CMC | - | - | - | 99.6 ± 0.1 |
| PorphSR_CMC_Gly | 3.07 ± 0.23 | 415.40 ± 2.03 (b),(h) | 3.95 ± 0.01 (b),(h) | 99.7 ± 0.1 |
| PorphSR_PcT | - | - | - | 99.7 ± 0.0 |
| PorphSR_PcT_Gly | 5.70 ± 0.63 (f) | 628.16 ± 8.62 (b),(f) | 6.05 ± 0.06 (b),(f),(h) | 99.9 ± 0.0 |
| Reference commercial film | 0.83 ± 0.02 (b),(c),(f),(h) | 3.4 ± 0.06 (b),(c),(f),(h) | 0.32 ± 0.01 (b),(c),(f),(h) | 0.0 ± 0.0 (a)-(h) |
| No film | 11.73 ± 0.61 (b),(c),(f),(h),(i) | - | - | - |

WVTR: water vapor transmission rate; WVP: water vapor permeability. Uncovered silica gel. Statistically significant differences between (a) PorphSR, (b) PorphSR_Gly, (c) PorphSR_PcT, (d) PorphSR_PcT_Gly, (e) PorphSR_CMC, (f) PorphSR_CMC_Gly, (g) PorphSR_AL, (h) PorphSR_AL_Gly, and (i) the commercial film.

All produced materials are highly susceptible to water, a common feature of films derived from natural polymers [37]. While the reference commercial film is not soluble in water at room temperature, almost all produced materials promptly dissolved (Table 4). Solubility values in water were above 99.6%, except for the PorphSR_AL system (around 98.8%) ($p < 0.05$) and were apparently higher in films containing glycerol compared to the same compositions without plasticizers (Table 4), although no statistically significant differences were found (Appendix A).

3.5. Mechanical Performance

Figure 9 shows the tensile curves for both the produced films and a standard commercial film; Table 5 displays the resulting apparent Young’s modulus, ultimate tensile strength, and fracture strain values for the produced materials. Using the Bonferroni pairwise comparison tool, statistically significant differences between film samples were identified using indexes *a* to *h*. In Appendix B (Tables A5–A7), the full statistical analysis for the obtained values is shown. The statistical significance of some of the identified film compositions’ influences was not verified. Increasing the number of tested samples in future studies should solve this limitation. For all formulations, UTS corresponds to the fracture stress, with most films displaying brittle behavior. The UTS value of the PorphSR film was around 13 MPa (Figure 9a, black line).

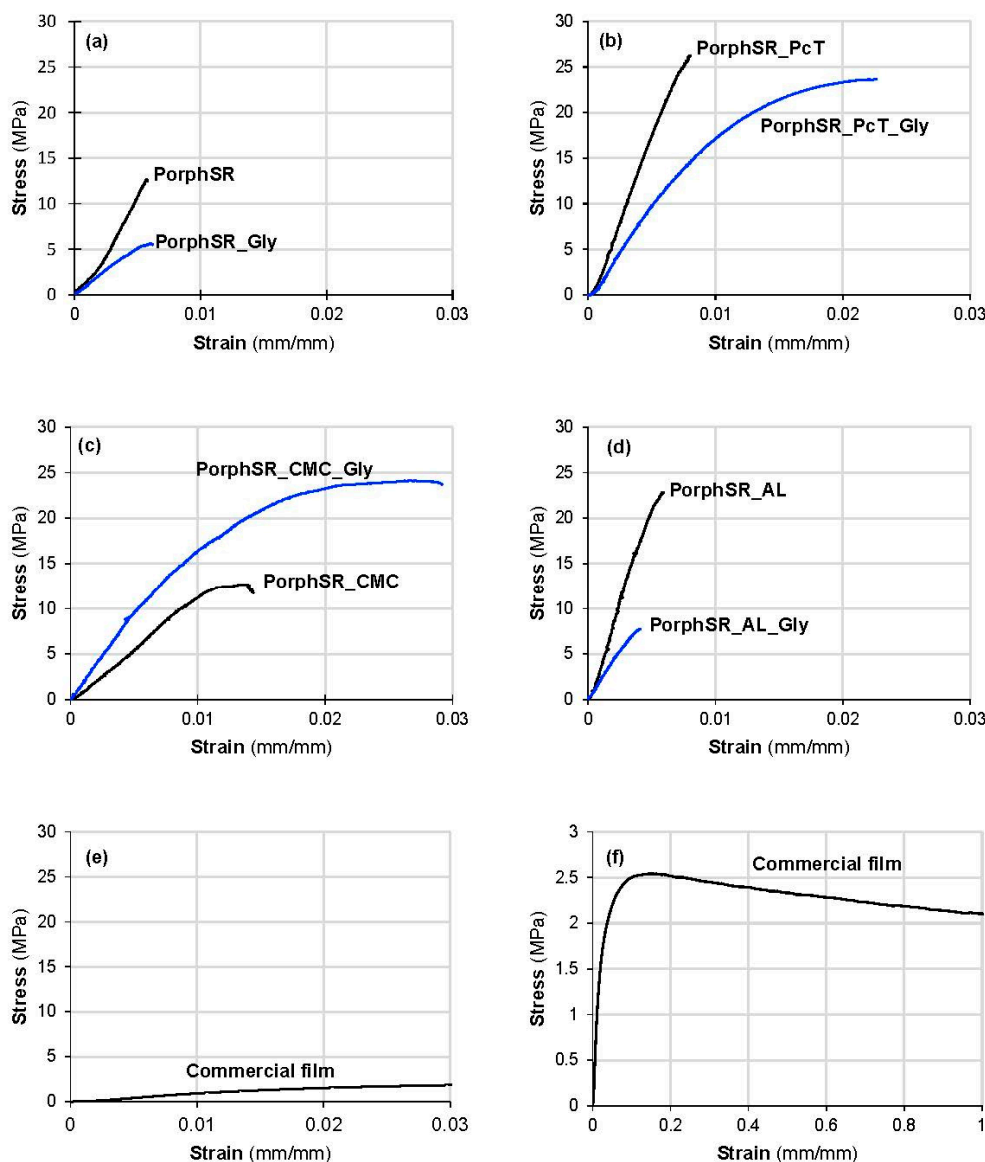


Figure 9. Tensile curves obtained for (a) PorphSR and PorphSR_Gly, (b) PorphSR_PcT and PorphSR_PcT_Gly, (c) PorphSR_CMC and PorphSR_CMC_Gly, (d) PorphSR_AL and PorphSR_AL_Gly, and (e,f) the commercial reference film, using different scales. (Blue line: films containing glycerol.)

Table 5. Apparent Young's modulus, UTS, and fracture strain average values obtained for the produced films and the reference commercial material.

| | E' (GPa) | UTS (MPa) | ϵ_f (%) |
|-----------------|-----------------------------|---------------------------|-------------------------|
| PorphSR | 2.90 ± 0.52 | 12.9 ± 0.8 | 0.53 ± 0.20 |
| PorphSR_Gly | 1.12 ± 0.20 (a) | 4.3 ± 0.8 | 0.41 ± 0.14 |
| PorphSR_PcT | 3.99 ± 0.27 (a),(b) | 26.0 ± 5.9 (a),(b) | 0.82 ± 0.25 |
| PorphSR_PcT_Gly | 1.62 ± 0.14 (a),(c) | 23.2 ± 1.6 (b) | 2.94 ± 0.74 (a)-(c) |
| PorphSR_CMC | 1.62 ± 0.33 (a),(c) | 10.3 ± 2.6 (c),(d) | 0.90 ± 0.48 (d) |
| PorphSR_CMC_Gly | 1.65 ± 0.30 (a),(c) | 21.9 ± 4.3 (b),(e) | 3.10 ± 0.80 (a)-(c),(e) |
| PorphSR_AL | 4.21 ± 0.19 (a),(b),(d)-(f) | 17.4 ± 5.0 (b) | 0.52 ± 0.20 (d),(f) |
| PorphSR_AL_Gly | 1.58 ± 0.42 (a),(c),(g) | 9.3 ± 3.0 (c),(d),(f) | 0.75 ± 0.23 (d),(f) |
| Commercial film | 0.08 ± 0.00 (a)-(h) | 2.5 ± 0.1 (c),(d),(f),(g) | n.a. |

E': apparent Young's modulus; UTS: ultimate tensile stress; ϵ_f : fracture strain. Statistically significant differences between (a) PorphSR, (b) PorphSR_Gly, (c) PorphSR_PcT, (d) PorphSR_PcT_Gly, (e) PorphSR_CMC, (f) PorphSR_CMC_Gly, (g) PorphSR_AL, and (h) PorphSR_AL_Gly.

UTS's value was differently affected by the presence of a second polysaccharide in the formulation, increasing to around 17 MPa in PorphSR_AL (Figure 9d, black line) and to 26 MPa in PorphSR_PcT (Figure 9a, black line). No statistically significant evidence was found in the first case, but evidence ($p = 0.01167$) of the increase was found for the second case. This was accompanied by an increase in the material ductility of PorphSR_PcT (ϵ_f increased around 56% compared to PorphSR); the presence of alginate appeared to have no influence upon ductility, although no statistically significant evidence was found ($p > 0.05$). In addition, the E' value for PorphSR was around 2.9 GPa, increasing to 4.2 GPa in PorphSR_AL ($p = 0.00017$) and to 4.0 in PorphSR_PcT ($p = 0.00344$) (Table 5). The opposite effects resulted from the presence of CMC (Figure 9c, black line): UTS and E' decreased to around 10 MPa and 1.6 GPa, respectively, accompanied by a ϵ_f increase of approximately 56% compared to PorphSR, although only strong statistically significant evidence of these influences was found for the E' decrease ($p = 0.00344$). Adding glycerol plasticizer to PorphSR (Figure 9a, blue line) decreased the UTS and E' values, but also decreased ϵ_f (Table 5). Importantly, adding glycerol increased the plastic component of the deformation in the PorphSR_PcT, PorphSR_CMC, and PorphSR_AL films (Figure 9b–d, respectively). In both PorphSR_PcT_Gly and PorphSR_CMC_Gly, ϵ_f reached around 3% (approximately 3.5-fold increase compared to the corresponding films without glycerol); in PorphSR_AL_Gly, it reached 0.75% (1.4-fold increase), but no statistically significant evidence was found. This was accompanied by a decrease in E' (from 4.0 GPa in PorphSR_PcT to 1.6 GPa in PorphSR_PcT_Gly; from 4.2 GPa in PorphSR_AL to 1.6 GPa in PorphSR_PcT_Gly) ($p < 0.001$) and in UTS (from 26 MPa in PorphSR_PcT to 23 MPa in PorphSR_PcT_Gly; from 17 MPa in PorphSR_AL to 9 MPa in PorphSR_PcT_Gly), without statistically significant evidence being observed. However, the addition of glycerol had no statistically significant effect ($p > 0.05$) upon the apparent modulus of PorphSR_CMC (1.6 GPa).

Figure 9e shows the mechanical performance of the reference commercial film under the same deformation regime imposed on the produced materials, displaying an E' value of 82.4 MPa (35-fold lower than the base PorphSR material). Strong or very strong statistically significant evidence of this difference ($p < 0.01$) between all films and the reference commercial film was found. Figure 9f additionally shows the performance of the commercial film up to 100% tensile strain, which reached a UTS of 2.5 MPa (five-fold lower than PorphSR ($p = 0.06465$)). These low E' and UTS values were accompanied by very high fracture strain values, with fracture points still to be reached at 250% tensile strain (when the equipment limit was achieved). Localized plastic deformation onset at UTS corresponded to tensile strain of about 12%.

4. Discussion

In this work, porphyrin-based edible films previously prepared by the gelation and drying of food-grade suspensions [8] were characterized in terms of their mechanical and physical abilities for use as food packaging.

Porphyrin gelation is based on the conformational transition of the randomly coiled polymer chains (Figure 1) to ordered double helix structures [10,21] is possible when the electrostatic repulsion between porphyrin chains is sufficiently low to allow their association by hydrophobic interactions and electrostatic interactions via hydroxyl groups [2,10,21]. Gelation is a physical process and does not need any additional reactive species [21]; nonetheless, blending with another polysaccharide is a simple and convenient method used to obtain different film properties and to prepare new compositions [10]. For this purpose, the formulated filmogenic suspensions included blends with glycerol as a plasticizer and/or alginate, pectin, and carboxymethylcellulose polysaccharide [8], the aim being to enhance film properties compared to those based on individual porphyrin [10].

The structures of porphyrin-based films produced from polysaccharides by gelation are expected to result from a mechanism whereby the conformational change of either polymer is independent of the presence of the other [10]. Therefore, the polysaccharide mixture must be homogenized above the constituent polysaccharides' melting temperature, such that, on cooling, independent crosslinking takes place in the filmogenic solution [38]. This results in an interpenetrating solid network at room temperature, without phase separation [38,39]. Furthermore, the mechanical and physical properties of films obtained from the gelation and drying of polysaccharide mixtures depend on the polysaccharides' individual properties and their proportion in the mixtures [38]. Film performance is expected to be dominated by the most abundant ingredient [38], which in the current study is always the second polysaccharide blended with porphyrin (Table 2). Structure-wise, the properties of the 3D network formed directly depend on the number of links and, eventually, on the degree of aggregation of the double-chain segments [38].

Overall, the results of the mechanical tests (Table 5) showed that the produced materials were fragile, stiff, and brittle, with fracture strain values between approximately 0.4 and 3%, depending on composition (Figure 9a–d). Fracture strain is a measure of material ductility, and these values were much higher than that of the reference commercial film, with ϵ_f above 250% (Figure 9f). The base PorphSR film displayed ductility values around 0.5%, accompanied by E' and UTS values around 2.9 GPa and 12.9 MPa, respectively. The presence of a second polysaccharide in the formulation increased the ductility of PorphSR-PcT and PorphSR_CMC films, but not PorphSR_AL (with no alteration in ϵ_f values compared to PorphSR), and increased UTS, except for PorphSR_CMC. Brittle behavior is typical in packaging produced from natural polysaccharide gels [18,22] due to extensive interactions between polymeric chains (mainly hydrogen, hydrophobic, disulfide, and electrostatic interactions) [4]. The addition of a plasticizer is usually necessary to improve the mechanical properties (increasing flexibility, stretchability, and toughness), ensuring package integrity during the full chain, from production through to storage and distribution [4]. For this purpose, glycerol, a common plasticizer agent often used in edible film formulations, was added to the porphyrin-based formulations [4,22,40]. The obtained results indicated that, except for the base formulation (PorphSR), the presence of plasticizer increased the fracture strain by up to three times, rendering films with increased ductility compared with the corresponding compositions without plasticizers (Table 5). This was accompanied by a decrease in the values of the apparent Young's modulus for all films except PorphSR_CMC_Gly (the values for which remained unaltered) and by UTS decrease for all films except PorphSR_CMC_Gly. Despite this improvement in plastic behavior, the mechanical performances of the produced materials were much lower than that of the reference commercial film (Figure 9f). In practice, only films with glycerol are sufficiently ductile to withstand manipulation and forming operations (§3.5). Glycerol's effect as a plasticizer is due to the ability of its small-chain-size molecules to position themselves between polysaccharide chains, increasing the free volume between

them [40]; it is also favored by the additional plasticizing effect of excess water absorbed by glycerol (which is lower in films containing pectin; Figure 3) [18]. The resulting decrease in intermolecular forces weakens polymer–polymer interactions, resulting in less crosslinking and the increased mobility of polymer chains [40]. For this reason, overall material plasticity increases, expectedly and is accompanied by lower E' and UTS [22,40,41]. While a lower apparent modulus is advantageous with respect to film behavior (decreasing stiffness), a lower UTS can be detrimental (leading to fracture at lower imposed stresses). UTS and elongation at break are the two most important mechanical properties for food packaging films (both edible natural polymers and common plastics); acceptable performance requires a UTS between 1 and 10 MPa and a ϵ_f between 1 and 10% (ideally these values should be 10-fold higher) [22]. While the achieved ductility values were poor (ϵ_f below 1%) for most films, they were in line with fracture strain values reported in the literature for Ca-caseinate/glycerol, polystyrene, and chia seed mucilage films, for example [22,42]. On the other hand, the PorphSR_PcT_Gly and PorphSR_CMC_Gly films achieved around 3% fracture strain—an acceptable performance [22]—similar to those of methylcellulose, hydroxypropyl methylcellulose, whey protein isolate/beeswax/glycerol, konjac glucomannan/curdlan, and chia seed mucilage/glycerol films [22,42,43]. Regarding UTS, most formulations (apart from PorphSR_Gly and PorphSR_AL_Gly) performed above the 10 MPa reference barrier [22], reaching up to 26 MPa. This is in line with common plastics, such as low- and high-density polyethylene, polypropylene and polystyrene, and edible films, such as whey protein isolate/glycerol, fish myofibrillar protein/glycerol, corn zein/glycerol, and high-amylose pea starch/glycerol films [22].

The importance of plasticizer addition in ensuring film functionality is also indicated by the failure of films produced without glycerol when deformed to test their barrier ability against water vapor (§3.5). For this reason, only materials containing glycerol could be assessed. All tested films displayed significantly higher permeability values than the reference commercial film (Table 4), which was to be expected considering the highly hydrophilic character of polysaccharides [2]. Compared to PorphSR_Gly, water barrier properties were enhanced in films containing CMC, while they decreased when alginate or pectin was used as the second polysaccharide in the blend (Figure 8, Table 4). This is in good agreement with the films' composition, the fraction of the second polysaccharide present always being higher than that of porphyran (Table 2). In fact, film properties depend on the individual properties and proportions of the two polysaccharides in the formulation and are expected to be most strongly determined by the most abundant ingredient [38], while carboxymethylcellulose has been reported to display a high water barrier ability, contrarily to the poor performances of alginate and pectin [2,22]. Acceptable water vapor barrier performance requires a permeability between 1 and 10 $\text{mm}\cdot\text{g}\cdot\text{m}^2\cdot\text{d}^{-1}\cdot\text{kPa}^{-1}$ [22]—a range achieved by all the glycerol-added films, especially PorphSR_Gly and PorphSR_CMC_Gly. This permeability range is in line with values obtained for cellophane (regenerated cellulose), wheat gluten/glycerol, wheat gluten/beeswax/glycerol, whey protein isolate/beeswax/sorbitol, whey protein isolate/beeswax/glycerol, and Ca-caseinate/beeswax films [22]. Ideally, the WVP of food packaging film should be in the order of 0.1 $\text{mm}\cdot\text{g}\cdot\text{m}^2\cdot\text{d}^{-1}\cdot\text{kPa}^{-1}$ or below [22], as achieved by the reference commercial film (0.32 $\text{mm}\cdot\text{g}\cdot\text{m}^2\cdot\text{d}^{-1}\cdot\text{kPa}^{-1}$). However, although the barrier and mechanical performance values of the produced materials were lower than those of the reference commercial film, they apparently ensured adequate film integrity. Ultimately, their suitability as packaging materials depends on the response to the envisaged food contents [1,2]: the shelf life of chocolate cereal balls—a dry food with a high lipid content—is mostly limited by lipid oxidation (leading to flavor alteration) and water absorption (leading to reduced crispness) [8]. In this context, a previous sensory analysis comparing conventionally packed cereals and cereals packed in the produced films showed no perceptible difference in taste or crispness [8], which also confirmed that the films offer adequate barrier protection for the requirements of the envisaged food packaging application.

The resulting films are transparent (Figure 2)—a useful property in food packaging since it allows the consumer to see through it to the goods inside [37]. Optical transparency requires that the material has a uniform index of refraction [44], for which the high miscibility of the porphyrin/polysaccharide filmogenic solution and the structural homogeneity and uniformity of the crosslinked structure are mandatory [44]. This indicates the absence of phase separation [38] in the interconnected network formed by the independent gelation of each polysaccharide during crosslinking, cooling from gelation temperature [38], and during water removal on drying [39].

Consistent with their optical transparency, the films displayed amorphous structures (Figure 6). Since polymer diffraction plots are additive [24], the absence of individual phase peaks superimposed in the diffractograms of porphyrin blends with glycerol and/or the second polysaccharide confirmed the high miscibility of the phases. Furthermore, the introduction of glycerol further enhanced the miscibility of the individual phases, giving rise to new structures and increasing film homogeneity. This is expected to have resulted from the positioning of glycerol molecules between polymer chains, thus increasing the free volume of the polymer structure and overall molecular mobility [22]. This leads to enhancement of the amorphous region and the suppression of crystallite [10].

The base PorphSR film (Figure 3a) displayed the most uniform microstructure and the smoothest surface among all the produced films. Film surface roughness successively increased when CMC, pectin, or alginate were present in the formulations, both without (Figures 3a and 2a–d) and with (Figures 3a–e and 2a–h) glycerol. This was expected to result from the viscosity increase in the filmogenic solution when a second polysaccharide was present [24] compared to the corresponding porphyrin-only base solution. Since the more viscous the solution, the more difficult the release of gaseous by-products formed during gelation, more gas bubbles remain entrapped in the formed solid and contribute to film roughness [24,41]. On the other hand, the surface roughness of the films without glycerol (Figure 4a, dashed line) were always higher than those of the corresponding film compositions with glycerol (Figure 4a, full line). This was because the addition of a plasticizer reduces intermolecular forces and increases the mobility of polymer chains, leading to viscosity decrease [41], which results in increased composition uniformity and fewer entrapped bubbles [24]. For the same reason, the addition of glycerol appeared to decrease film thickness (Figure 4b, full line) compared to compositions without plasticizers (Figure 4b, dashed line). Film thickness varied between approximately 30 and 44 μm with the presence of glycerol and between around 28 and 43 μm in the glycerol-free blends. These values are an order of magnitude lower than the measured thickness of the reference commercial film ($393.3 \pm 4.1 \mu\text{m}$).

The density values of the produced materials ranged between 1.45 and 1.63 g/cm^3 in compositions without glycerol plasticizers (Figure 4c, dashed line). In the corresponding compositions with glycerol (Figure 4c, full line), density values were lower, ranging between 1.37 and 1.61 g/cm^3 . This is expected to have resulted from glycerol's ability to position itself between polymer molecules, interfering with polymer–polymer interactions to maintain greater distances between polymer chains, thus leading to less efficient volume occupation. The attained values were in good agreement with values calculated using the rule of mixtures, while they were 40 to 70% higher than the measured density value of the reference commercial film ($0.96 \pm 0.4 \text{ g}/\text{cm}^3$). Nevertheless, because the thickness of the reference film was much higher, package weights were approximately five times higher than those for the developed materials (for the same package area). Given this, the replacement of conventional polymeric films with the developed films would result in lower net weights, which should correspond to lower transportation costs and emissions.

Contrarily to the reference commercial film (Figure 7j, dashed line), the produced materials are sensitive to heat (Figure 7a–h). Submitting materials to increasing temperatures progressively softens and then destroys the molecular arrangements of the polymer backbones. The presence of glycerol affects the temperature values at which these thermal events take place (Figure 7i). Glass transition was especially affected: softening

onset ranged from 45 to 57 °C (depending on film composition) in the films without glycerol and decreased to 31–40 °C when glycerol was present (corresponding to a decrease between 13 and 39%, depending on composition), because of the associated reductions in intermolecular forces and increase in free volume and chain mobility [22,41]. T_g values were in good agreement with the films' brittle behavior at room temperature (§3.6). The decrease in brittleness in the presence of glycerol shows the plasticizer effect: glycerol molecules interfere with polymer–polymer crosslinking by positioning themselves between polymer molecules [40] and thus decreasing the degree of cure of the thermoset [4]. Again, this improves the films' flexibility and ductility at room temperature and the overall material thermoplasticity [22,41]. It should also be mentioned that the existence of a single glass transition event confirms the miscibility of the polysaccharide blends in porphyran films [10,14]. Additionally, none of the mixtures displayed a peak corresponding to the melting transition, again confirming their amorphous structure and thermoset nature [33,36]. As temperature increases, decomposition of the porphyran polysaccharide takes place, starting with the random breaking of glycosidic bonds, followed by glycosidic breakage, oxidative decomposition, and thermal decomposition [34,35,45–47]. Glycosidic breakage onset was detected between 167 and 185 °C, depending on the second polysaccharide present in the blend (Figure 7i), but was almost independent of the presence of glycerol. These thermal transitions are irreversible (as shown by the absence of structural recovery on cooling), again indicating the thermoset nature of the produced polymers [33].

The produced materials are also sensitive to humidity and showed total or very high solubility in water (Table 4). Hydrodegradability is a common phenomenon in films derived from natural polymers [18], resulting from their high hydrophilicity [2,22]. Similarly, materials with glycerol are more soluble than their counterparts without plasticizers [18].

Although polymer degradation under the influence of heat or hydrolysis during use is undesirable, it is very useful in the context of prevention of environmental pollution [1,35,41]. Contrarily to conventional thermosets, the produced materials can be treated at low temperature or (preferably) be dissolved [4] after use: when used as food enclosures, they can be disposed of either by eating them or by dissolution; if they are disposed of in landfill or end up in nature, they will rapidly dissolve under the action of the elements, without leaving any toxic residues [4].

5. Conclusions

In this work, biodegradable edible films based on porphyran were characterized. The results showed that by adding glycerol plasticizers and/or a second polysaccharide (alginate, pectin, or carboxymethylcellulose) it is possible to enhance film properties compared to those based on porphyran alone. In the absence of glycerol, film properties are expected to be determined by the most abundant polysaccharide, which is, in all formulations, the one added to the base porphyran solution. All produced films are homogeneous, transparent, and slightly colored. In addition, the materials' structure is amorphous and crosslinked, confirming them as thermosets. The addition of CMC, alginate, or pectin to the porphyran-based formulation appeared to slightly decrease the materials' solubility in water, the ability to incorporate water in the film structure, and the temperature for the onset of glass transition. This is expected to result from less effective crosslinking in the resulting interconnected structure, either because of the lower number of junctions or the lower degree of chain segment aggregation compared to porphyran-only films. For the same reason, the presence of the second polysaccharide decreased the apparent Young's modulus and ultimate tensile strength values (except for carboxymethylcellulose), accompanied by a slight increase in ductility. However, the achieved ductility enhancement was not sufficient to reach the accepted standard values required for food packaging. Compliance with these values requires the addition of a plasticizer to the filmogenic solutions. The use of glycerol plasticizers increased the materials' solubility in water and the amount of absorbed water and decreased the temperature of glass transition onset compared to the corresponding compositions without glycerol. Glycerol was also effective

in enhancing the mechanical properties of the films, decreasing stiffness and resistance and significantly increasing ductility. In particular, porphyran/pectin/glycerol and porphyran/carboxymethylcellulose/glycerol films displayed sufficiently high ductility values to be used as food packaging. Furthermore, their water vapor barrier characteristics were sufficiently high to prevent excessive moisture transport to food contents. Given this, the studied porphyran/pectin/glycerol and porphyran/carboxymethylcellulose/glycerol films displayed a combination of physical and mechanical properties that would ensure adequate film integrity and function through the complete food packaging supply chain. Further study is required: an improvement in ductility and permeability values above at least 10% is demanded to surpass the mentioned standards. Nevertheless, these results present an opportunity to extend the scope of porphyran films to applications in the dry food packaging industry.

Author Contributions: Conceptualization: M.G., R.S.B., S.B., R.B. and C.A. Data curation: M.G. and R.S.B. Formal analysis: A.C.F., S.E., M.G., R.S.B., S.B., R.B. and C.A. Funding acquisition: A.C.F., M.G., R.B., S.B., R.B. and C.A. Investigation: M.G., R.S.B., A.C.F., S.E., M.T. and P.A. Methodology: M.G., R.S.B. and S.B. Project administration: A.C.F., M.G., R.S.B., C.A., R.B. and S.B. Resources: A.C.F., M.G., R.S.B., C.A., R.B. and S.B. Supervision: S.B. and M.G. Validation: M.G., R.B., S.B., R.B. and C.A. Writing—original draft: M.G. and R.S.B. Writing—review and editing: A.C.F., M.G., R.S.B., C.A., R.B., S.B. and P.A. All authors have read and agreed to the published version of the manuscript.

Funding: This work was supported by national funds through the Fundação para a Ciência e Tecnologia (FCT); through project UIDB/04540/2020 granted to CeFEMA, project UIDB/50022/2020 granted to IDMEC, and project LA/P/0069/2020 granted to the associate laboratory ARNET. FCT funding also includes projects UIDB/04292/2020 and UIDP/04292/2020 granted to MARE. This study received financial support from the Instituto Politécnico de Setúbal.

Institutional Review Board Statement: Not applicable.

Informed Consent Statement: Not applicable.

Data Availability Statement: The data that support the findings of this study are available from the corresponding author upon request.

Acknowledgments: The authors thank the Lisbon Biomechanics Laboratory (LBL) at Instituto Superior Técnico and Sérgio Gonçalves for carrying out the tensile tests.

Conflicts of Interest: The authors declare no conflict of interest.

Appendix A. Interactions with Water

The features of films' interaction with water were statistically analyzed. One-way ANOVA combined with the Bonferroni pairwise comparison tool was used to determine statistically significant evidence of differences between films. Very strong statistically significant evidence ($p < 1.2 \times 10^{-15}$) of differences between series were found for all properties.

Tables A1–A4 show the Bonferroni pairwise p -values obtained for the films' water interaction properties.

Table A1. Bonferroni pairwise comparison p -values for the different desiccant mass gains.

| | PorphSR_Gly | PorphSR_AL_Gly | PorphSR_CMC_Gly | PorphSR_PcT_Gly | Commercial Film |
|-----------------|-----------------------|-----------------------|-----------------------|-----------------------|-----------------------|
| PorphSR_AL_Gly | 1 | - | - | - | - |
| PorphSR_CMC_Gly | 1 | 1 | - | - | - |
| PorphSR_PcT_Gly | 9.39×10^{-2} | 7.01×10^{-1} | 1.74×10^{-2} | - | - |
| Commercial film | 1.05×10^{-2} | 1.70×10^{-3} | 5.49×10^{-2} | 7.02×10^{-5} | - |
| No film | 2.93×10^{-7} | 7.81×10^{-7} | 1.35×10^{-7} | 7.42×10^{-6} | 9.70×10^{-9} |

Table A2. Bonferroni pairwise comparison *p*-values for the different water vapor transmission rates.

| | PorphSR_Gly | PorphSR_AL_Gly | PorphSR_CMC_Gly | PorphSR_PcT_Gly |
|-----------------|------------------------|------------------------|------------------------|------------------------|
| PorphSR_AL_Gly | 2.00×10^{-10} | - | - | - |
| PorphSR_CMC_Gly | 1.10×10^{-2} | 5.40×10^{-11} | - | - |
| PorphSR_PcT_Gly | 4.50×10^{-10} | 2.98×10^{-1} | 1.10×10^{-10} | - |
| Commercial film | 7.90×10^{-14} | 1.90×10^{-15} | 1.50×10^{-13} | 2.40×10^{-15} |

Table A3. Bonferroni pairwise comparison *p*-values for the different water vapor permeabilities.

| | PorphSR_Gly | PorphSR_AL_Gly | PorphSR_CMC_Gly | PorphSR_PcT_Gly |
|-----------------|------------------------|------------------------|------------------------|------------------------|
| PorphSR_AL_Gly | 3.20×10^{-13} | - | - | - |
| PorphSR_CMC_Gly | 1.50×10^{-07} | 7.30×10^{-12} | - | - |
| PorphSR_PcT_Gly | 1.80×10^{-12} | 2.00×10^{-05} | 8.30×10^{-11} | - |
| Commercial film | 7.80×10^{-12} | 1.40×10^{-15} | 3.40×10^{-13} | 3.60×10^{-15} |

Table A4. Bonferroni pairwise comparison *p*-values for the different solubilities.

| | PorphSR | PorphSR_Gly | PorphSR_AL | PorphSR_AL_Gly | PorphSR_CMC | PorphSR_CMC_Gly | PorphSR_PcT | PorphSR_PcT_Gly |
|-----------------|-----------------------|-----------------------|-----------------------|----------------------|----------------------|----------------------|----------------------|----------------------|
| PorphSR_Gly | 1 | - | - | - | - | - | - | - |
| PorphSR_AL | 4.10×10^{-2} | 4.10×10^{-2} | - | - | - | - | - | - |
| PorphSR_AL_Gly | 1 | 1 | 1 | - | - | - | - | - |
| PorphSR_CMC | 1 | 1 | 5.71×10^{-1} | 1 | - | - | - | - |
| PorphSR_CMC_Gly | 1 | 1 | 3.33×10^{-1} | 1 | 1 | - | - | - |
| PorphSR_PcT | 1 | 1 | 2.50×10^{-1} | 1 | 1 | 1 | - | - |
| PorphSR_PcT_Gly | 1 | 1 | 5.90×10^{-1} | 1 | 1 | 1 | 1 | - |
| Commercial film | $<2 \times 10^{-16}$ | $<2 \times 10^{-16}$ | $<2 \times 10^{-16}$ | $<2 \times 10^{-16}$ | $<2 \times 10^{-16}$ | $<2 \times 10^{-16}$ | $<2 \times 10^{-16}$ | $<2 \times 10^{-16}$ |

Appendix B. Statistical Analysis of Mechanical Properties

The films' apparent Young's moduli, ultimate tensile strengths, and fracture strains were statistically analyzed. The Shapiro–Wilk normality test was applied to all samples, and evidence of normal distribution was found ($p > 0.05$). Therefore, the parametric one-way ANOVA was combined with the Bonferroni pairwise comparison tool to determine statistically significant evidence of differences between them. Very strong statistically significant evidence ($p < 6e^{-9}$) of differences between series were found for all properties.

Tables A5–A7 show the Bonferroni pairwise *p*-values obtained for the films' apparent Young's moduli, ultimate tensile strengths, and fracture strains, respectively. $p < 0.001$, 0.01, and 0.05 indicate very strong, strong, and evidence of statistically significant differences between film samples.

Table A5. Bonferroni pairwise comparison *p*-values for the different films' apparent Young's moduli.

| | PorphSR | PorphSR_Gly | PorphSR_PcT | PorphSR_PcT_Gly | PorphSR_CMC | PorphSR_CMC_Gly | PorphSR_AL | PorphSR_AL_Gly |
|-----------------|------------------------|------------------------|------------------------|------------------------|------------------------|------------------------|------------------------|-----------------------|
| PorphSR_Gly | 1.60×10^{-6} | - | - | - | - | - | - | - |
| PorphSR_PcT | 3.44×10^{-3} | 1.30×10^{-12} | - | - | - | - | - | - |
| PorphSR_PcT_Gly | 2.19×10^{-3} | 1.0 | 4.10×10^{-9} | - | - | - | - | - |
| PorphSR_CMC | 8.50×10^{-4} | 1.0 | 5.60×10^{-10} | 1 | - | - | - | - |
| PorphSR_CMC_Gly | 1.10×10^{-3} | 8.99×10^{-1} | 7.10×10^{-10} | 1 | 1 | - | - | - |
| PorphSR_AL | 1.70×10^{-4} | 6.40×10^{-14} | 1 | 2.60×10^{-10} | 2.80×10^{-10} | 3.50×10^{-11} | - | - |
| PorphSR_AL_Gly | 5.00×10^{-4} | 1 | 3.50×10^{-10} | 1 | 1 | 1 | 1.80×10^{-11} | - |
| Commercial film | 2.00×10^{-10} | 2.25×10^{-3} | 1.90×10^{-15} | 4.30×10^{-5} | 1.20×10^{-5} | 9.10×10^{-6} | $<2 \times 10^{-16}$ | 2.10×10^{-5} |

Table A6. Bonferroni pairwise comparison *p*-values for the different films' ultimate tensile strengths.

| | PorphSR | PorphSR _Gly | PorphSR _PcT | PorphSR _PcT_Gly | PorphSR _CMC | PorphSR _CMC_Gly | PorphSR _AL | PorphSR _AL_Gly |
|-----------------|-----------------------|-----------------------|-----------------------|-----------------------|-----------------------|-----------------------|------------------------|-----------------------|
| PorphSR_Gly | 2.18×10^{-1} | - | - | - | - | - | - | - |
| PorphSR_PcT | 1.17×10^{-2} | 1.34×10^{-2} | - | - | - | - | - | - |
| PorphSR_PcT_Gly | 1.16×10^{-1} | 1.62×10^{-5} | 1 | - | - | - | - | - |
| PorphSR_CMC | 1 | 1 | 1.32×10^{-3} | 1.41×10^{-2} | - | - | - | - |
| PorphSR_CMC_Gly | 1.32×10^{-1} | 4.33×10^{-6} | 1 | 1 | 1.26×10^{-2} | - | - | - |
| PorphSR_AL | 1 | 2.90×10^{-4} | 1.51×10^{-1} | 1 | 5.82×10^{-1} | 1 | - | - |
| PorphSR_AL_Gly | 1 | 1 | 2.30×10^{-4} | 2.92×10^{-3} | 1 | 1.85×10^{-3} | 1.33×10^{-1} | - |
| Commercial film | 6.47×10^{-2} | 1 | 6.70×10^{-7} | 7.03×10^{-6} | 5.44×10^{-1} | 2.07×10^{-4} | $<1.00 \times 10^{-4}$ | 7.29×10^{-1} |

Table A7. Bonferroni pairwise comparison *p*-values for the different films' fracture strains.

| | PorphSR | PorphSR _Gly | PorphSR _PcT | PorphSR _PcT_Gly | PorphSR _CMC | PorphSR _CMC_Gly | PorphSR _AL |
|-----------------|-----------------------|-----------------------|-----------------------|-----------------------|-----------------------|-----------------------|----------------|
| PorphSR_Gly | 1 | - | - | - | - | - | - |
| PorphSR_PcT | 1 | 1 | - | - | - | - | - |
| PorphSR_PcT_Gly | 5.39×10^{-7} | 9.00×10^{-8} | 5.65×10^{-6} | - | - | - | - |
| PorphSR_CMC | 1 | 1 | 1 | 1.04×10^{-5} | - | - | - |
| PorphSR_CMC_Gly | 1.55×10^{-7} | 2.60×10^{-8} | 1.51×10^{-6} | 1 | 2.72×10^{-6} | - | - |
| PorphSR_AL | 1 | 1 | 1 | 1.19×10^{-7} | 1 | 3.30×10^{-8} | - |
| PorphSR_AL_Gly | 1 | 1 | 1 | 3.10×10^{-6} | 1 | 8.42×10^{-7} | 1 |

References

- Marsh, K.; Bugusu, B. Food Packaging—Roles, Materials, and Environmental Issues. *J. Food Sci.* **2007**, *72*, 39–55. [[CrossRef](#)] [[PubMed](#)]
- Kumar, L.; Ramakanth, D.; Akhila, K.; Gaikwad, K.K. Edible Films and Coatings for Food Packaging Applications: A Review. *Environ. Chem. Lett.* **2022**, *20*, 875–900. [[CrossRef](#)]
- Raheem, D. Application of Plastics and Paper as Food Packaging Materials—An Overview. *Emirates J. Food Agric.* **2017**, *25*, 177–188. [[CrossRef](#)]
- Hamed, I.; Jakobsen, A.N.; Lerfall, J. Sustainable Edible Packaging Systems Based on Active Compounds from Food Processing Byproducts: A Review. *Compr. Rev. Food Sci. Food Saf.* **2022**, *21*, 198–226. [[CrossRef](#)]
- Marangoni Júnior, L.; Jamróz, E.; Gonçalves, S.d.Á.; da Silva, R.G.; Alves, R.M.V.; Vieira, R.P. Preparation and Characterization of Sodium Alginate Films with Propolis Extract and Nano-SiO₂. *Food Hydrocoll. Health* **2022**, *2*, 100094. [[CrossRef](#)]
- Mohamed, S.A.A.; El-Sakhawy, M.; El-Sakhawy, M.A.-M. Polysaccharides, Protein and Lipid-Based Natural Edible Films in Food Packaging: A Review. *Carbohydr Polym.* **2020**, *238*, 116178. [[CrossRef](#)]
- Anderson, N.S.; Rees, D.A. Porphyrin: A Polysaccharide with a Masked Repeating Structure. *J. Chem. Soc.* **1965**, 5880–5887. [[CrossRef](#)]
- Teles, M.; Adão, P.; Afonso, C.; Bernardino, R.; Guedes, M.; Baptista, R.; Bernardino, S. Development and Characterization of Films for Food Application Incorporating Porphyrin Extracted from *Porphyra dioica*. *Coatings* **2022**, *12*, 148. [[CrossRef](#)]
- Morrice, L.M.; McLean, M.W.; Long, W.F.; Williamson, F.B. Porphyrin Primary Structure. *Hydrobiologia* **2004**, *116–117*, 572–575.
- Bhatia, S.; Namdeo, A.G.; Nanda, S. Factors Effecting the Gelling and Emulsifying Properties of a Natural Polymer. *Syst. Rev. Pharm.* **2010**, *1*, 86–92. [[CrossRef](#)]
- Fernando, S.; Kim, K.-N.; Kim, D.; Jeon, Y.-J. Algal Polysaccharides: Potential Bioactive Substances for Cosmeceutical Applications. *Crit. Rev. Biotechnol.* **2019**, *39*, 99–113. [[CrossRef](#)] [[PubMed](#)]
- Rees, D.A.; Conway, E. The Structure and Biosynthesis of Porphyrin: A Comparison of Some Samples. *Biochem. J.* **1962**, *84*, 411–416. [[CrossRef](#)] [[PubMed](#)]
- Jung, H.; Yoon, W.B.; Matsukawa, S. Effect of Moisture Uptake on the Texture of Dried Laver *Porphyra*. (Nori) Studied by Mechanical Characterization and NMR Measurements. *Food Hydrocoll.* **2022**, *124*, 107223. [[CrossRef](#)]
- Bhatia, S.; Sharma, K.; Nagpal, K.; Bera, T. Investigation of the Factors Influencing the Molecular Weight of Porphyrin and Its Associated Antifungal Activity. *Bioact. Carbohydr. Diet. Fibre* **2015**, *5*, 153–168. [[CrossRef](#)]
- Cassani, L.; Lourenço-Lopes, C.; Barral-Martinez, M.; Chamorro, F.; Garcia-Perez, P.; Simal-Gandara, J.; Prieto, M.A. Thermochemical Characterization of Eight Seaweed Species and Evaluation of Their Potential Use as an Alternative for Biofuel Production and Source of Bioactive Compounds. *Int. J. Mol. Sci.* **2022**, *23*, 2355. [[CrossRef](#)]
- Sinurat, E.; Fransiska, D.; Livia. The Effect of Addition Glycerol Against Nori Characterization from *Gracilaria* sp. and *Ulva* sp. Seaweeds. *IOP Conf. Ser. Earth Environ. Sci.* **2021**, *715*, 12054. [[CrossRef](#)]

17. Adão, P.; Reboleira, J.; Teles, M.; Santos, B.; Ribeiro, N.; Teixeira, C.M.; Guedes, M.; Pessoa, J.C.; Bernardino, S. Enhancement of the Antioxidant and Antimicrobial Activities of Porphyrin through Chemical Modification with Tyrosine Derivatives. *Molecules* **2021**, *26*, 2916. [[CrossRef](#)]
18. Cian, R.E.; Salgado, P.R.; Drago, S.R.; Mauri, A.N. Effect of Glycerol and Ca²⁺ Addition on Physicochemical Properties of Edible Carrageenan/Porphyrin-Based Films Obtained from the Red Alga, *Pyropia Columbina*. *J. Appl. Phycol.* **2015**, *27*, 1699–1708. [[CrossRef](#)]
19. Cian, R.E.; Alaiz, M.; Vioque, J.; Drago, S.R. Enzyme Proteolysis Enhanced Extraction of ACE Inhibitory and Antioxidant Compounds (Peptides and Polyphenols) from *Porphyra Columbina* Residual Cake. *J. Appl. Phycol.* **2013**, *25*, 1197–1206. [[CrossRef](#)]
20. Nieto, M.B. Structure and Function of Polysaccharide Gum-Based Edible Films and Coatings. In *Edible Films and Coatings for Food Applications*; Embuscado, M.E., Huber, K.C., Eds.; Springer: New York, NY, USA, 2009; pp. 57–112.
21. Beaumont, M.; Tran, R.; Vera, G.; Niedrist, D.; Rousset, A.; Pierre, R.; Shastri, V.P.; Forget, A. Hydro-gel-Forming Algae Polysaccharides: From Seaweed to Biomedical Applications. *Biomacromolecules* **2021**, *22*, 1027–1052. [[CrossRef](#)]
22. Han, J.H. Chapter 9—Edible Films and Coatings: A Review. In *Food Science and Technology*, 2nd ed.; Han, J.H., Ed.; Academic Press: San Diego, CA, USA, 2014; pp. 213–255, ISBN 978-0-12-394601-0.
23. Begum, R.; Yusof, Y.A.; Aziz, M.G.; Uddin, M.B. Structural and Functional Properties of Pectin Extracted from Jackfruit (*Artocarpus heterophyllus*) Waste: Effects of Drying. *Int. J. Food Prop.* **2017**, *20*, S190–S201. [[CrossRef](#)]
24. Klug, H.P.; Alexander, L.E. *X-ray Diffraction Procedures: For Polycrystalline and Amorphous Materials*, 2nd ed.; Wiley: New York, NY, USA, 1974.
25. Kanmani, P.; Rhim, J.-W. Antimicrobial and Physical-Mechanical Properties of Agar-Based Films Incorporated with Grapefruit Seed Extract. *Carbohydr. Polym.* **2014**, *102*, 708–716. [[CrossRef](#)] [[PubMed](#)]
26. Cazón, P.; Morales-Sanchez, E.; Velazquez, G.; Vázquez, M. Measurement of the Water Vapor Permeability of Chitosan Films: A Laboratory Experiment on Food Packaging Materials. *J. Chem. Educ.* **2022**, *99*, 2403–2408. [[CrossRef](#)]
27. Abdel-Galil, A.; Ali, H.E.; Atta, A.; Balboul, M.R. Influence of Nanostructured TiO₂ Additives on Some Physical Characteristics of Carboxymethyl Cellulose (CMC). *J. Radiat. Res. Appl. Sci.* **2014**, *7*, 36–43. [[CrossRef](#)]
28. Jia, S.; Yu, D.; Zhu, Y.; Wang, Z.; Chen, L.; Fu, L. Morphology, Crystallization and Thermal Behaviors of PLA-Based Composites: Wonderful Effects of Hybrid GO/PEG via Dynamic Impregnating. *Polymers* **2017**, *9*, 528. [[CrossRef](#)]
29. Suryadi, H.; Sutriyo; Fauziah, G. Characterization Sodium Carboxymethyl Cellulose from Alpha Cellulose Betung Bamboo (*Dendrocalamus asper*). *Pharmacogn. J.* **2019**, *11*, 894–900. [[CrossRef](#)]
30. Zhu, J.; Li, Q.; Che, Y.; Liu, X.; Dong, C.; Chen, X.; Wang, C. Effect of Na₂CO₃ on the Microstructure and Macroscopic Properties and Mechanism Analysis of PVA/CMC Composite Film. *Polymers* **2020**, *12*, 453. [[CrossRef](#)]
31. Hu, W.; Chen, S.; Wu, D.; Zheng, J.; Ye, X. Ultrasonic-Assisted Citrus Pectin Modification in the Bicarbonate-Activated Hydrogen Peroxide System: Chemical and Microstructural Analysis. *Ultrason. Sonochem.* **2019**, *58*, 104576. [[CrossRef](#)]
32. Bhagyaraj, S.; Krupa, I. Alginate-Mediated Synthesis of Hetero-Shaped Silver Nanoparticles and Their Hydrogen Peroxide Sensing Ability. *Molecules* **2020**, *25*, 435. [[CrossRef](#)]
33. Hammer, A.; Fedelich, N.; Giani, S.; Hempel, E.; Jing, N.; Nijman, M.; Riesen, R.; Schawe, J.; Schubnell, M. *Thermal Analysis of Polymers*; Mettler-Toledo: Greifensee, Switzerland, 2013.
34. Motta, M.V.L.; de Castro, E.V.R.; Muri, E.J.B.; Loureiro, B.V.; Costalonga, M.L.; Filgueiras, P.R. Thermal and Spectroscopic Analyses of Guar Gum Degradation Submitted to Turbulent Flow. *Int. J. Biol. Macromol.* **2019**, *131*, 43–49. [[CrossRef](#)]
35. Qiu, Y.; Jiang, H.; Fu, L.; Ci, F.; Mao, X. Porphyrin and Oligo-Porphyrin Originating from Red Algae *Porphyra*: Preparation, Biological Activities, and Potential Applications. *Food Chem.* **2021**, *349*, 129209. [[CrossRef](#)] [[PubMed](#)]
36. Argon, A. *The Physics of Deformation and Fracture of Polymers*; Cambridge University Press: Cambridge, UK, 2013; pp. 1–511. [[CrossRef](#)]
37. Cian, R.E.; Salgado, P.R.; Drago, S.R.; González, R.J.; Mauri, A.N. Development of Naturally Activated Edible Films with Antioxidant Properties Prepared from Red Seaweed *Porphyra Columbina* Biopolymers. *Food Chem.* **2014**, *146*, 6–14. [[CrossRef](#)] [[PubMed](#)]
38. Rinaudo, M. Gelation of Polysaccharides. *J. Intell. Mater. Syst. Struct.* **1993**, *4*, 210–215. [[CrossRef](#)]
39. Simoni, R.C.; Lemessandra, G.F.; Fialho, S.; Gonçalves, O.H.; Gozzo, A.M.; Chiaradia, V.; Sayer, C.; Shirai, M.A.; Leimman, F.V. Effect of Drying Method on Mechanical, Thermal and Water Absorption Properties of Enzymatically Crosslinked Gelatin Hydrogels. *Eng. Sci. An. Acad. Bras. Ciênc* **2017**, *89* (Suppl. 1), 745–755. [[CrossRef](#)] [[PubMed](#)]
40. Mellinas, C.; Valdés, A.; Ramos, M.; Burgos, N.; del Carmen Garrigós, M.; Jiménez, A. Active Edible Films: Current State and Future Trends. *J. Appl. Polym. Sci.* **2016**, *133*, 42631. [[CrossRef](#)]
41. Kibar, E.A.A.; Ferhunde, U. Thermal, Mechanical and Water Adsorption Properties of Corn Starch–Carboxymethylcellulose/Methylcellulose Biodegradable Films. *J. Food Eng.* **2013**, *114*, 123–131. [[CrossRef](#)]
42. Dick, M.; Costa, T.M.H.; Gomaa, A.; Subirade, M.; Rios, A.D.O.; Flôres, S.H. Edible Film Production from Chia Seed Mucilage: Effect of Glycerol Concentration on Its Physicochemical and Mechanical Properties. *Carbohydr. Polym.* **2015**, *130*, 198–205. [[CrossRef](#)]
43. Wu, C.; Peng, S.; Wen, C.; Wang, X.; Fan, L.; Deng, R.; Pang, J. Structural Characterization and Properties of Konjac Glucomannan/Curdlan Blend Films. *Carbohydr. Polym.* **2012**, *89*, 497–503. [[CrossRef](#)]
44. Fox, M. *Optical Properties of Solids*; Oxford University Press: Oxford, UK, 2002.

45. Wang, S.; Xia, Z.; Hu, Y.; He, Z.; Uzoejinwa, B.B.; Wang, Q.; Cao, B.; Xu, S. Co-Pyrolysis Mechanism of Seaweed Polysaccharides and Cellulose Based on Macroscopic Experiments and Molecular Simulations. *Bioresour. Technol.* **2017**, *228*, 305–314. [[CrossRef](#)]
46. Wang, S.; Hu, Y.; Uzoejinwa, B.B.; Cao, B.; He, Z.; Wang, Q.; Xu, S. Pyrolysis Mechanisms of Typical Seaweed Polysaccharides. *J. Anal. Appl. Pyrolysis* **2017**, *124*, 373–383. [[CrossRef](#)]
47. Wang, S.; Xia, Z.; Wang, Q.; He, Z.; Li, H. Mechanism Research on the Pyrolysis of Seaweed Polysaccharides by Py-GC/MS and Subsequent Density Functional Theory Studies. *J. Anal. Appl. Pyrolysis* **2017**, *126*, 118–131. [[CrossRef](#)]